remote sensing

IMPACT FACTOR 5.349

CITESCORE 7.4

Review

Imaging Cultural Heritage at Different Scales: Part I, the Micro-Scale (Manufacts)

Luca Piroddi, Nasser Abu Zeid, Sergio Vincenzo Calcina, Patrizia Capizzi, Luigi Capozzoli, Ilaria Catapano, Marilena Cozzolino, Sebastiano D'Amico, Rosa Lasaponara and Deodato Tapete

Special Issue

Remote, Proximal Sensing and Geophysics for Cultural Heritage Knowledge and Conservation

Edited by

Dr. Luca Piroddi, Dr. Nasser Abu Zeid, Dr. Patrizia Capizzi, Dr. Marilena Cozzolino, Dr. Sebastiano D'Amico, Dr. Sergio Vincenzo Calcina, Dr. Ilaria Catapano and Dr. Rosa Lasaponara

MDPI

https://doi.org/10.3390/rs15102586

remote sensing

MDPI

Review

Imaging Cultural Heritage at Different Scales: Part I, the Micro-Scale (Manufacts)

Luca Piroddi [1,2,*], Nasser Abu Zeid [3], Sergio Vincenzo Calcina [1], Patrizia Capizzi [4], Luigi Capozzoli [5], Ilaria Catapano [6], Marilena Cozzolino [7], Sebastiano D'Amico [2], Rosa Lasaponara [5] and Deodato Tapete [8]

1 Department of Civil, Environmental Engineering and Architecture, University of Cagliari, Via Marengo 2, 09123 Cagliari, Italy; sergiocalcina@virgilio.it
2 Department of Geosciences, University of Malta, 2080 MSD Msida, Malta; sebastiano.damico@um.edu.mt
3 Department of Physics and Earth Sciences, University of Ferrara, Via Saragat 1, 44122 Ferrara, Italy; a.nasser@unife.it
4 Department of Earth and Sea Sciences, University of Palermo, Via Archirafi, 22, 90123 Palermo, Italy; patrizia.capizzi@unipa.it
5 Institute of Methodologies for Environmental Analysis, National Research Council of Italy (IMAA CNR), C. da S. Loja—Zona Industriale, Tito Scalo, 85050 Potenza, Italy; luigi.capozzoli@imaa.cnr.it (L.C.); rosa.lasaponara@imaa.cnr.it (R.L.)
6 Institute for Electromagnetic Sensing of the Environment, National Research Council of Italy (IREA CNR), Via Diocleziano 328, 80127 Napoli, Italy; catapano.i@irea.cnr.it
7 Department of Agricultural, Environmental and Food Sciences, University of Molise, Via De Sanctis snc, 86100 Campobasso, Italy; marilena.cozzolino@unimol.it
8 Italian Space Agency (ASI), Via del Politecnico snc, 00133 Rome, Italy; deodato.tapete@asi.it
* Correspondence: lucapiroddi@yahoo.it

Abstract: Applications of non-invasive sensing techniques to investigate the internal structure and surface of precious and delicate objects represent a very important and consolidated research field in the scientific domain of cultural heritage knowledge and conservation. The present article is the first of three reviews focused on contact and non-contact imaging techniques applied to surveying cultural heritage at micro- (i.e., manufacts), meso- (sites) and macro-scales (landscapes). The capability to infer variations in geometrical and physical properties across the inspected surfaces or volumes is the unifying factor of these techniques, allowing scientists to discover new historical sites or to image their spatial extent and material features at different scales, from landscape to artifact. This first part concentrates on the micro-scale, i.e., inspection, study and characterization of small objects (ancient papers, paintings, statues, archaeological findings, architectural elements, etc.) from surface to internal properties.

Keywords: proximal sensing; micro-geophysics; non-destructive diagnostics; imaging techniques; cultural heritage

Citation: Piroddi, L.; Abu Zeid, N.; Calcina, S.V.; Capizzi, P.; Capozzoli, L.; Catapano, I.; Cozzolino, M.; D'Amico, S.; Lasaponara, R.; Tapete, D. Imaging Cultural Heritage at Different Scales: Part I, the Micro-Scale (Manufacts). *Remote Sens.* **2023**, *15*, 2586. https://doi.org/10.3390/rs15102586

Academic Editor: Mercedes Solla

Received: 14 April 2023
Revised: 10 May 2023
Accepted: 11 May 2023
Published: 15 May 2023

1. Introduction

Conservation science of cultural heritage is nowadays a multidisciplinary research field, where remote sensing techniques play a key role, first of all owing to their capability of allowing the inspection of the surface and internal structure of fragile objects with high artistic and economic value without, or with very minimal, contact.

Therefore, non-invasive techniques provide a fundamental toolkit to achieve an improved understanding and documentation of the physical, chemical and aesthetic properties of cultural heritage, to provide heritage bodies with the objective knowledge needed not only to unveil how these objects were produced and preserved over time, but also to assure future conservation and exhibition in safety conditions.

While the use of such techniques for diagnostic purposes has a long history, it is only in quite recent times that the technological advancement in sensors and instrumentation

has enabled the customization of methods to inspect small targets such as individual architectural elements or decorative finishes of historical buildings, paintings, statues or ancient papers. Therefore, techniques that initially were not exploited for the study of cultural heritage due to their intrinsic technical limitations have been proven suitable for these purposes and are now part of the portfolio of instrumental techniques that are increasingly used in conservation science. In some cases, the contribution of the so-called micro-geophysical methods, jointly with proximal sensing techniques, is still relevant to knowledge and documentation of cultural sites or manufacts. Especially for very thin targets, proximal sensing techniques are very feasible methods to be chosen.

At all scales of implementation, i.e., micro- (manufacts), meso- (sites) and macro-scales (landscapes), the current trend is to integrate different diagnostic techniques, according to the principle that each technique has specific features and capabilities to offer, and only their combination would lead to the achievement of the intended study objectives. This approach nowadays applies to different tasks in the lifecycle of cultural heritage study and conservation, including data collection, processing, visualization, interpretation, data fusion, scenario reconstruction, virtual fruition and musealization, virtual restoration, hazard reduction, preservation and repair actions.

This article is part of a solicited editorial project within the Special Issue "*Remote, Proximal Sensing and Geophysics for Cultural Heritage Knowledge and Conservation*" of the journal "Remote Sensing" and aims to review the various scales of non-invasive diagnostics applied to cultural heritage assets, through the provision of a brief summary of the working principles and mechanisms of each "family" of techniques and a demonstration via selected case studies. The article attempts to outline the main advantages and specifics of some of the most-used diagnostic methods at different scales, as evidenced by real-world implementation.

The present article is the first of three review papers focusing on the three implementation scales. This first paper concentrates on the micro-scale, i.e., inspection, study and characterization, from surface to internal properties, of small objects, including, but not limited to, ancient papers, paintings, statues, archaeological findings and architectural elements, and is organized into two main sections as follows:

Section 2: Proximal Sensing

2.1. X-ray radiography;
2.2. Ultraviolet induced fluorescence;
2.3. Infrared reflectography, photography and thermography;
2.4. Multi spectral imaging;
2.5. Hyperspectral imaging;
2.6. Terahertz imaging;
2.7. Integrated techniques.

Section 3: Micro-geophysics

3.1. Micro-seismic, sonic and ultrasonic surveys;
3.2. Electrical surveys;
3.3. Electromagnetic methods;
3.4. Architectural elements case studies;
3.5. Statues case studies;
3.6. Small archaeological features case studies.

2. Proximal Sensing

Proximal sensing techniques denote several non-invasive technologies in which the target objects—in the present context, cultural heritage manufacts—are placed within a short distance of the sensor, detector or camera lens collecting the data. Depending on the technology employed and the study purpose, the sensors/detectors work in different portions of the electromagnetic spectrum, from X-ray to ultraviolet (UV), from visible (VIS) to infrared (IR) and, further, from microwave to radio (Figure 1). For the sake of simplicity, these techniques may be divided into "spot" and "imaging" methodologies.

Examples of spot methodologies include X-ray fluorescence (XRF) spectroscopy, Fourier transform infrared (FT-IR) spectroscopy and fiber-optic reflectance spectroscopy (FORS). On the contrary, ultraviolet-induced fluorescence (UVF), infrared reflectography (IRR) and infrared photography (IRP), X-ray radiography (XRR) [1–6], multi-spectral imaging (MSI), hyperspectral imaging (HSI) and time-domain terahertz imaging (THz-TDI) are examples of imaging methodologies, naming only a few of the most-employed ones [7–18].

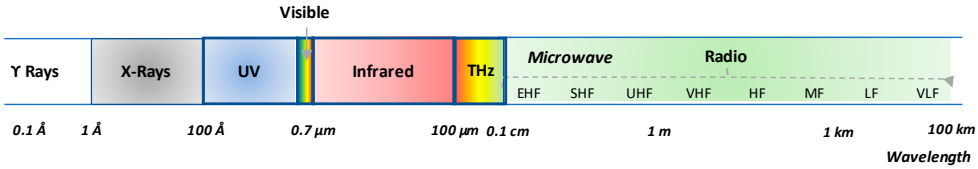

Figure 1. Portions of the electromagnetic spectrum exploited by proximal sensing technology for cultural heritage investigations.

A large number of case studies assessing the advantages and limitations of every single technique and the potentialities offered by their hierarchical employment have been reported in the literature [19].

Leaving aside spot methodologies, this section gives a brief overview of the most widely used active imaging technologies, starting from those working at very high frequencies, such as X-ray and ultraviolet (UV), moving to those at terahertz (THz) frequencies.

2.1. X-ray Radiography (XRR)

X-ray Radiography (XRR) is among the oldest and most-standardly employed non-destructive inspection technologies [20]. XRR exploits ionizing electromagnetic signals whose wavelength ranges between 1 and 250 pm (picometer, 10^{-12} m) and works in transmission mode, with the object under investigation located between the source and the detector. As the transmission of X-rays is inversely proportional to the density of the encountered materials, XRR is employed to achieve an insight into the inner structure of artwork. Moreover, since elements having high atomic weight, such as mercury (atomic number equal to 80), block the X-ray transmission, XRR is useful to discriminate pigments and inks containing such chemical elements.

Historically, XRR detectors have been designed to measure the intensity of the radiation only and thus suffer from internal noise, which constrains the achievable dynamic range, i.e., the number of collectable gray levels. As a consequence, continuous efforts have been made towards the development of novel detectors capable of enhancing XRR performance, so, today, a new generation of devices providing digital, color and high-resolution images are available [21]. Moreover, systems have been developed to scan tridimensional (3D) and/or large-size objects, thanks to the use of mechanical devices which allow for automatic motion of both the object and the detector [22,23].

Concerning the XRR imaging of large 3D objects, an interesting example is offered by the case study of "Doppio corpo", a wooden writing cabinet (studied by Pietro Piffetti) whose dimensions are 312 cm × 128 cm × 62 cm [24]. A novel prototype of computed tomography (CT) scanning was employed to obtain information about the inner structure of the masterpiece, its building technique, its conservation conditions and the presence of previous repairs and restorations. Specifically, the adopted CT prototype is made up of an X-ray source, a rotating platform—used to locate the object to be investigated—and a digital linear X-ray detector, scanning the projection plane using a high-precision mechanical system. The motion and the synchronization of the two moving parts as well as the data acquisition are regulated by two computers. Such CT devices and configurations overcome the size limits of characterizing the systems developed for medical purposes when used in the frame of CH for investigating objects such as mummies [25]. In this respect, recent advances in CT allow the totally non-invasive 3D reconstruction of the inner parts of inspected precious and delicate ancient goods, e.g., Figure 2 [26].

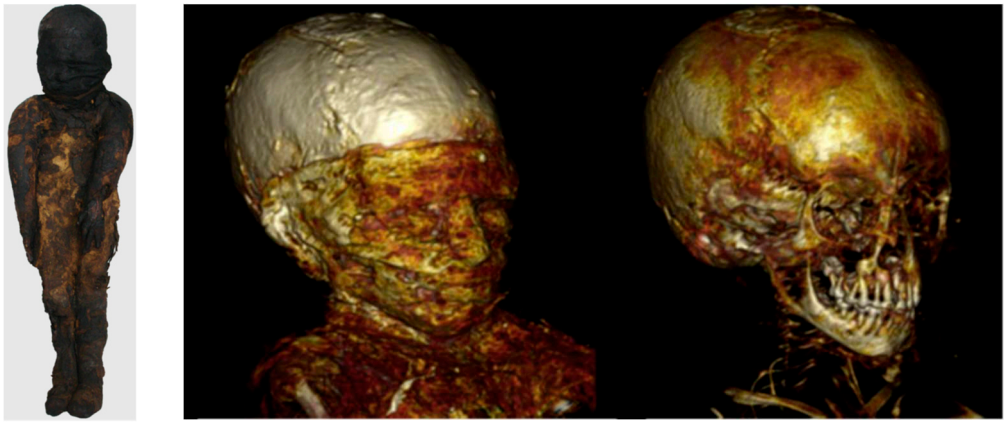

(**a**) (**b**) (**c**)

Figure 2. (**a**) Photograph of the bandaged ancient Egyptian child mummy from the Senckenberg Museum of Natural History in Frankfurt a.M. (inventory number ÄS 18). (**b**) 3D volume rendering illustrating hyperdense structures below the outer bandages, directly on the mummy's face, extending from the supraorbital margins to the chin and (**c**) the facial skeleton below [26].

2.2. Ultraviolet-Induced Fluorescence (UVF)

Fluorescence induced by UV radiation (UVF) is a common examination tool in artwork analysis because materials (especially organic materials) exhibit different fluorescence colors according to their chemical nature. UVF is an active imaging technique exploiting a source which emits in the UV region (100–400 nm wavelengths) and special photographic arrangements capable of acquiring the fluorescence signal. This signal is re-emitted from the materials after the molecular absorption of energy, which triggers the transition of the electrons to a higher electronic energy state [1,27].

UVF makes possible the localization of organic and inorganic materials (e.g., binders, colorants, pigments, etc.), the differentiation of materials with similar optical properties but different chemical composition (e.g., retouching, coatings and varnishes, added materials, etc.), the characterization of artwork condition, as well as the discrimination of repainted areas. In this regard, it is taken into account that the intensity of the fluorescence signal increases as the aging of materials proceeds [27–29].

One of the relevant examples regarding the employment of UVF for studying artwork deals with the study of Stradivari and Guarneri violins reported in [30], from which Figure 3 is taken. In this study, UVF was employed to gather information about the varnish thickness of three famous violins, specifically, the Stradivari "Toscano", the Stradivari "Ford" and the "Principe Doria" by Guarneri del Gesù, which were subject to minor, medium and major restoration actions. Specifically, it was observed that the UV color becomes darker when moving from the thickest to the thinnest varnished areas; thus, the most-worn portions of the violins could be detected. This was successfully verified for the well-preserved Stradivari Toscano violin, where each distinct fluorescent-colored area represented a different varnish thickness range and, therefore, represented a portion of the back plate of the violin with a specific conservation degree. Regarding the Ford violin, the UV imaging led to the hypothesis that a very thin UV-transparent over-polishing varnish was applied to the entire surface of the back plate. Finally, for the Guarneri del Gesù violin, it was found that the five differently UV-colored areas corresponded to three varnish strata of different thicknesses, which is maybe a consequence of the undocumented ordinary and extraordinary maintenance and restoration actions performed on this violin over time.

2.3. Infrared Reflectography (IRR), Photography (IRP) and Thermography (IRT)

IR radiation is widely used for artwork inspections and the technologies based on their use can be discriminated according to the frequency range at which they work. Indeed, the IR portion of the electromagnetic spectrum ranges from 0.7 µm up to 1 mm wavelengths

and it is divided into five sub-regions: near-infrared region (NIR; 0.7–1.1 μm), short-wave infrared (SWIR; 1.1–3 μm), mid-wave infrared (MWIR; 3–6 μm), long-wave infrared (LWIR; 6–15 μm) and extreme infrared region (15–100 μm), as shown in Figure 4.

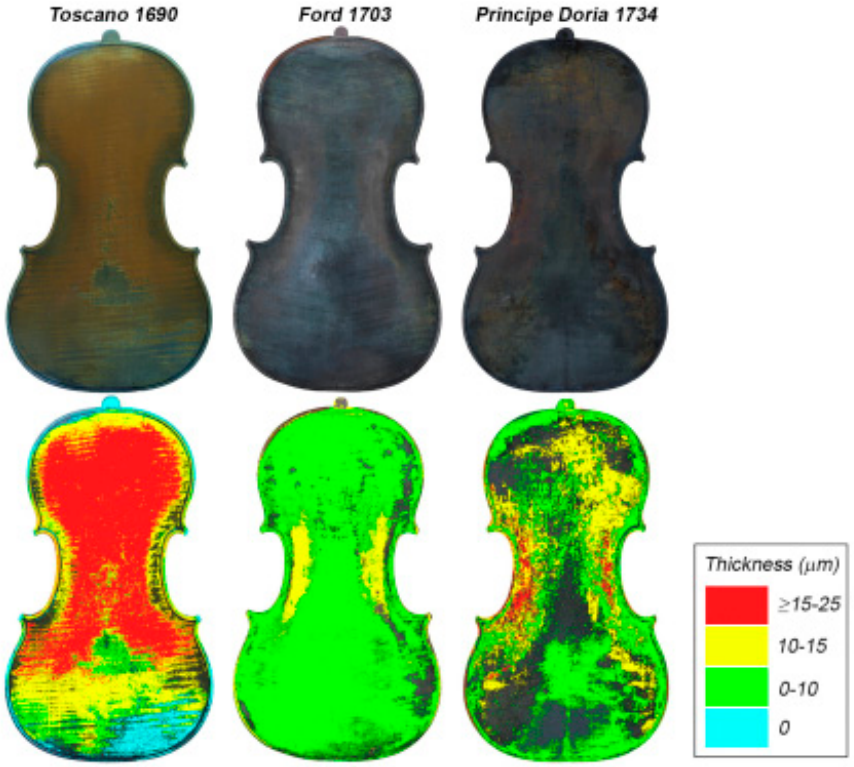

Figure 3. Photographs (**top**) and retrieved maps of varnish thickness (**bottom**) on the back plate of the Stradivari and Guarneri del Gesù violins [30].

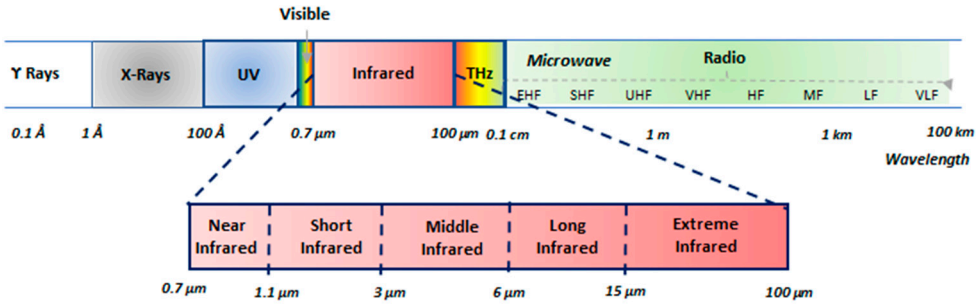

Figure 4. Wavelength partition of the infrared range.

Infrared reflectography (IRR) and infrared photography (IRP) work in the NIR region, typically exploiting 0.7–1.4 μm wavelengths, though there are devices exploiting wavelengths in the 1.5–3 μm range. Both IRR and IRP use an incandescent lamp, such as a halogen float lamp of 1000 W, or a quantum source, such as a light-emitting diode (LED) or laser, as a primary source and record the reflected radiation by means of a camera equipped with an infrared film (IRP) or a sensor sensitive to the infrared part of the spectrum (IRR) and an infrared cut-off filter [2,5,31]. The latter absorbs visible light and lets the infrared radiation pass. The commercially available IR-films are sensitive to radiation with a wavelength of up to 1.1 μm, while modern cameras can record IR radiation of wavelengths up to 2.4 μm. The gathered image, referred to as reflectogram, is not post-processed before interpretation.

In the NIR region, surface pictorial layers have an opacity that varies up to the point of becoming transparent and this depends on two main factors: the absorption of light by the pigment and the scattering of light by pigment particles, as detailed in [32].

Accordingly, IRR and IRP are frequently exploited to reveal the presence or absence of the preparatory design, the so-called "pentimenti" (changes from the initial design made by the artist during the painting process), or retouching and tampering on the work that can be attributed to previous restorations [33–35]. It is worth pointing out that revealing the presence of underdrawings and their relation to the final painting is a piece of valuable information to study the artist's technique and it can help art-historians to distinguish an original picture from a copy. However, the visibility of underdrawings depends on four parameters, two related to the material and the other two dependent on the adopted diagnostic instrumentation, as follows:

1. The difference between the reflectance of the materials used for the preparatory layer and of those used for the design (contrast factor);
2. The transparency of the pictorial material to the infrared radiation;
3. The sensitivity of the sensor;
4. The resolution capability of the detection system.

Active infrared thermography (IRT) accounts for the transient behavior of the artwork response to a thermal excitation; hence, it works mainly with long-wave (6–15 μm) infrared waves, which are thermal. IRT requires a suitable heating of the object, which is produced by the light emitted by flash or DC lamps, lasers or other light sources, and employs an infrared camera capable of recording the thermal radiation coming from the object under investigation. The output is a thermogram, i.e., a map allowing the identification of areas with different thermal diffusivity. Data processing of these maps in time-lapse, by means of properly designed software, enables the extraction of information about subsurface features and material inhomogeneities. In this regard, it is worth recalling that a homogeneous material is characterized by a uniform temperature distribution, while the presence of inhomogeneities, at or beneath the surface, can modify the heat propagation, resulting in localized thermal contrasts.

An issue with IRT is the duration of exposure to the heat source. Materials such as thick woods and metals can be subject to longer exposures and this allows for a longer time to study the heat exchange. Conversely, prolonged heat exposure can damage precious canvas paintings. In this case, a quick powerful flash is often considered to reduce the exposure time, but this allows a small window, 0.1–0.5 s, in which to record the temperature differential [36].

In the field of cultural heritage, IRT is used frequently to investigate both large objects, including monuments [37], portions of historical buildings [38] and ancient bridges [39], and small objects, such as books and documents, archaeological findings and artwork [40]. Regarding the latter category, interesting reviews are given in [41–43].

Thermographic inspection of panel paintings can be part of more complex protocols, including other diagnostic techniques [44,45]. Through active IRT, it is possible to collect very detailed evidence of subsurface features. For example, in Figure 5a, a typical experimental setup of pulsed thermography is shown, where the synchronization of IR flashes' energization and thermal camera acquisition achieves complete control of the experiment and obtains detailed diagnostic outputs, as in Figure 5d. The algorithm used here, pulsed phase thermography (PPT), is based on the fact that, mathematically, a pulse can be decomposed into a multitude of individual sinusoidal components; when a specimen is pulse heated, thermal waves of various amplitudes and frequencies are launched into the specimen and their properties can be reconstructed by extracting the various frequencies, with discrete one-dimensional Fourier transform, of each pixel (x,y) of the thermogram sequence [46].

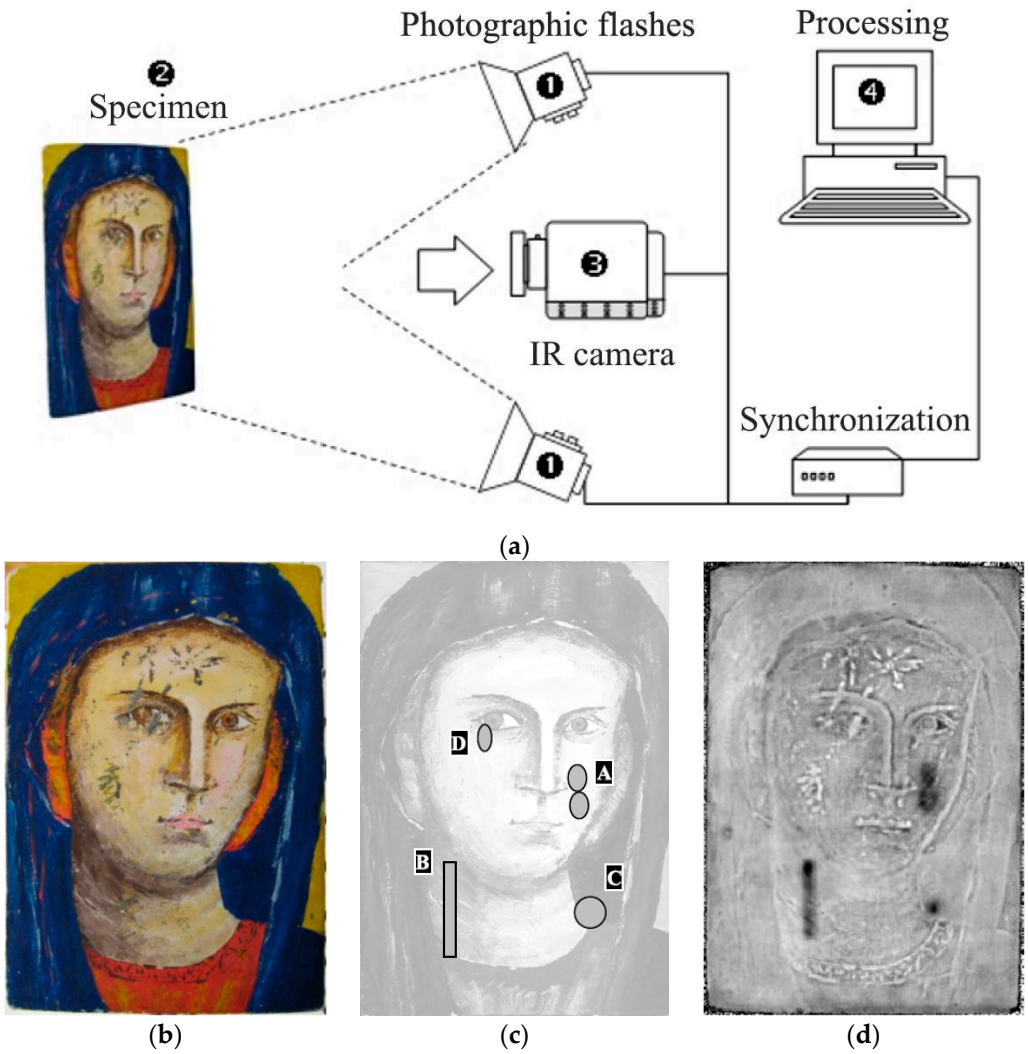

Figure 5. Subsurface artificial defects inspected by pulsed phase thermography (PPT): (**a**) experimental setup; (**b**) color photograph of the specimen; (**c**) image showing the localization of the 4 internal defects, indicated as A, B, C, and D; (**d**) processed result (phasegram) obtained by PPT [45].

When inspecting large surfaces of historical buildings, the energization from the sun is often used to perform active IRT acquisition over a long time interval. In similar configurations, Sfarra et al. [47] proposed a hybrid procedure combining concepts from PPT, thermographic signal reconstruction (TSR) and principal component thermography (PCT) to obtain quantitative information such as the defect depth. The authors tested their approach on the façade of the Santa Maria Collemaggio church (L'Aquila, Italy), wherein quantitative results related to the sub-superficial discontinuities were obtained thanks to the use of such advanced techniques (Figure 6). First, the time-lapse datasets were de-noised through their approximation by the first five to six elements of a logarithmic polynomic regression and then the filtered results were alternatively subject to the two processing steps (PPT or PCT). Introducing a characteristic frequency named f_{ch} [Hz] corresponding to the frequency of the first extreme (maximum or minimum) of the phase—or the amplitude—contrast, the z depth of the defect [m] can be retrieved:

$$z = f\left(\frac{\alpha}{f_{ch}}\right) \cong k_c\sqrt{\frac{\alpha}{f_{ch}}} \quad (1)$$

where α is the thermal diffusivity parameter [m^2/s]. The absolute phase contrast is as follows:

$$\Delta\emptyset = \emptyset_{defective} - \emptyset_{defect\text{-}free} \quad (2)$$

in which $\Phi_{defective}$ is the phase value for a defective area and $\Phi_{defect\text{-}free}$ is the phase value for a defined sound area.

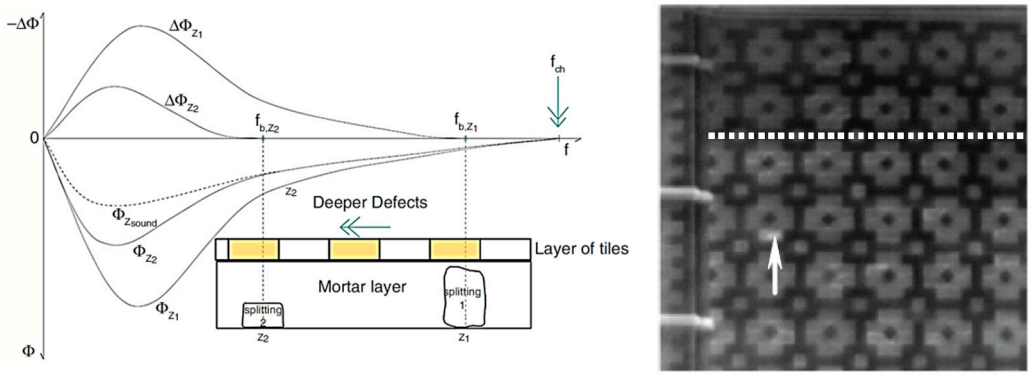

(**a**) (**b**)

Figure 6. Hybrid infrared thermography applied to the façade of the Santa Maria Collemaggio church: (**a**) general schematization applied for the detection of the f_{ch} value in reference to $\Delta\Phi$; (**b**) amplitudegram at f = 0.0054 Hz [47].

Another recent case study is the analysis of *La Primavera*, a 145 × 220 cm oil on canvas painting, realized by Mario Nuzzi and Filippo Lauri in 1658–59 and preserved in Palazzo Chigi (Ariccia, Italy) [48]. This masterpiece was investigated by means of reflectographic and thermographic techniques, which were used in a complementary way. First, an IR–ITR laser scanner prototype, developed at the ENEA Research Centre of Frascati (Rome, Italy), was employed to perform the preliminary and remote near-IR reflectographic survey of the areas where the canvas was located. Thereafter, the near-IR reflectographic map was used for planning the thermographic and mid-IR reflectographic studies, focusing the analyses on the most interesting areas of one of the paintings. The combination of the three imaging techniques revealed several details that were not otherwise visible by the naked eye; in particular, several pentimenti were detected that corresponded with the human figures. Figure 7 reports the results concerning Flora's face. Specifically, the IR–ITR image in Figure 7b reveals the presence of an additional face which does not appear in the visible image; the thermogram acquired with 20 ms delay barely shows the second Flora's profile (see Figure 7c), while the thermogram acquired at 300 ms delay reveals the structural pattern of the canvas (see Figure 7d). Finally, the MWIR reflectogram makes visible possible repaired defects in the preparatory layer and/or in the support (see Figure 7e).

2.4. Multispectral Imaging (MSI)

Multispectral imaging can be considered as the extension of white light imaging that captures several images of an object in a series of spectral bands, covering parts of the infrared and ultraviolet regions. This is performed by either using image sensors having multiple photodetectors for each pixel or adding a multispectral wheel which contains multiple optical band-pass filters for selecting different wavelength regions and then connecting to a conventional camera with a broadband response. The first technical solution implies that the image sensor changes with the spectral channels to be considered. Since the photodetectors cover certain spectral regions, the spectral data outside these regions are lost, causing a disadvantage in terms of achievable sensitivities. This drawback becomes more and more significant when the number of spectral channels increases and, thus, it is difficult to reach high performance and at the same time to cover a wide spectral region. The second technical solution offers the advantage of a simple selection of the

spectral ranges by continuously rotating the wheel or by using a computer control to select one filter at a time. Once the images are registered and calibrated, they are combined to form a reflectance image cube, where the images are represented by the X- and Y-axes and the Z-dimension denotes the wavelength of each image. Sometimes, Multi Images Stacking algorithms [49–51] are used to improve the outline details related to the artifact contents or to the conditions of the observed objects. In the field of artwork investigation, multispectral imaging is used to pursue two main goals. The first one is to obtain high color fidelity mainly of paintings, making them more readable; the second one is image spectroscopy, which allows for gathering information about the employed materials [52].

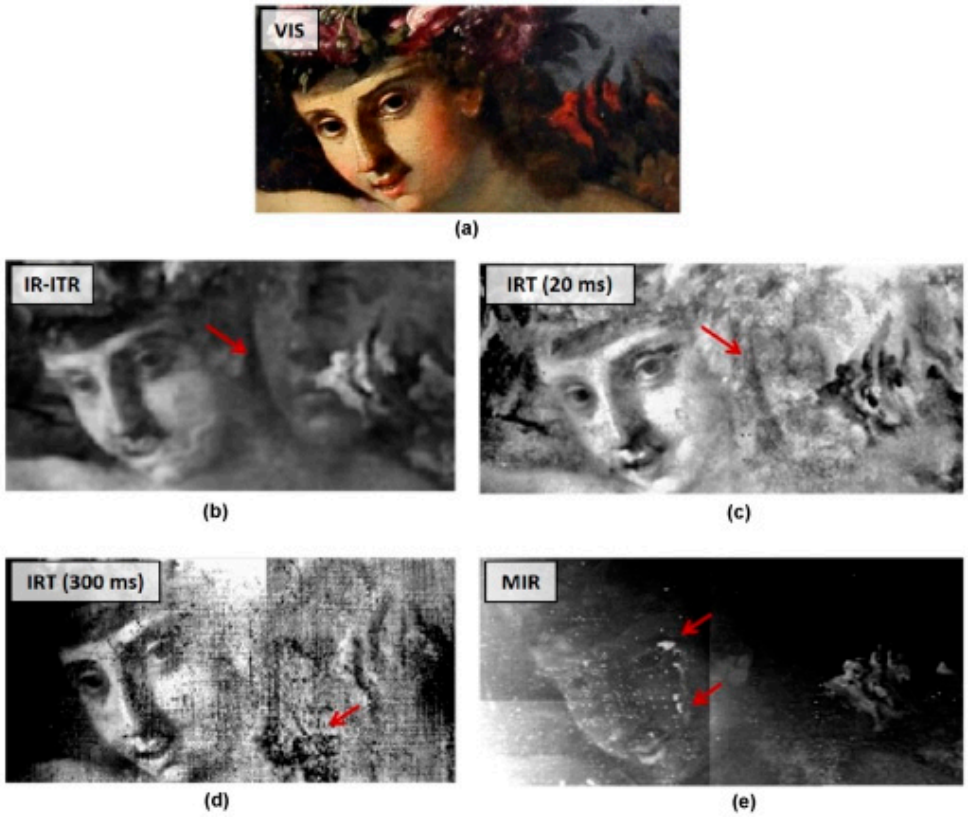

Figure 7. *La primavera* oil on canvas—Flora's face: (**a**) optical picture; (**b**) IR–ITR image; (**c**) corresponding thermogram acquired with 20 ms delay; (**d**) the thermogram acquired with 300 ms delay; (**e**) MWIR reflectogram [48]. The red arrows indicate elements or discontinuities not visible in the painting at visible light.

Multispectral datasets in the form of multispectral cubes can be processed with common image processing and fusion techniques to detect subtle details in painting [53]. In the cited reference, the authors proposed a processing workflow including a 2D wavelet decomposition of spectral—NIR—images, a histogram enhancing their high frequency spatial components and image fusion (removing the lowest frequency in NIR) to the visible datasets. The result is an image where the details (that were partially invisible due to painting deterioration or that are located immediately under the most recent painting layer) are revealed and made more readable (Figure 8).

The ability of NIR radiation to penetrate and reflect signals from the few upper layers of the inspected surfaces, jointly with the spectral signatures of inks, are the physical basis for the multispectral study of ancient books and palimpsests. With the appropriate choice of the energizing light, recording bands and pattern recognition methods, it is possible to distinguish and make readable two or more texts written on the same paper [54].

Figure 8. (**a**) Photograph, collected in the visible bands, of a vault pictorial scene and (**b**) the image resulting from the selection of NIR spatial high frequency data, their enhancement and fusion with the visible layer. The white arrows indicate the localization of a decorative element weakly visible at naked eye. Reprinted with permission from Piroddi et al. 2020 [53]. Copyright 2020 Springer Nature Switzerland AG.

2.5. Hyperspectral Imaging (HSI)

Hyperspectral imaging (HSI), also referred to as imaging spectrometry, uses a broadband light as its primary source, which illuminates the investigated object uniformly and collects hundreds of images at different wavelengths, mainly belonging to mid-infrared, near-infrared and visible segments of the electromagnetic spectrum [55]. Specifically, for each pixel of the observed scene, HSI detectors acquire data in contiguous and narrow bands, covering an extended spectral interval which depends on the adopted detector. Silicon (Si)-based sensors are capable of acquiring data in the 400–1000 nm range, indium gallium arsenide (InGaAs)-based sensors measure data at wavelengths ranging from 1000 nm up to 2500 nm, while cameras exploiting cooled indium antimonide (InSb)-based sensors work in the 1000–3000 nm range [34]. The collected data are arranged in a three-dimensional matrix, named hyperspectral cube, where two dimensions represent the spatial extent of the surveyed scene and the third-dimension accounts for the spectral content of the scene [56]. The spectral resolution of HSI data depends on the number of acquired bands and, thus, on the technical specifications of the instrumentation.

Several procedures can be used to process HSI data and allow for the visualization of concealed elements and details. Such details are not optically visible, as well as material identification according to their unique spectral signature. Moreover, multivariate analysis, such as PCA, and classification procedures are commonly exploited to generate new images that highlight the material distributions or details [57,58]. It is worth pointing out that the main issues are HSI noise, spectral mixing and huge data dimension [59]. Regarding the latter issue, techniques devoted to reducing data size have been proposed [60]. These techniques aim to choose a subset of wavelengths or their linear combinations by taking into account those wavelengths that carry the desired information for the pursued task of the survey.

In the field of artwork investigation, HSI is mainly used to perform non-invasive analysis of pigments, identify restored regions and reveal preparatory drawings [61]. Regarding HSI analysis of paintings, an example is the study reported in [62], regarding the study of two canvas paintings made by Picasso in 1917, specifically, *Blanquita Suárez* and *Woman in an armchair*. Both these pieces are exhibited in the Museum Picasso (Barcelona, Spain).

In the case of the *Blanquita Suárez* painting, HSI data allowed the documentation of the artist's technique; in particular, they revealed the preparatory drawing and evidenced that the artist used the intersection of lines and planes to realize the painting. In addition, HSI data made possible the detection of a modification, as corroborated by Figure 9a,b, which gives the sRGB image of the face of Blanquita Suárez (Figure 9a) and the corresponding SWIR image at 1350 nm (Figure 9b). The latter was extracted from the HSI cube-file. By comparing the left and right images in Figure 9a,b, it can be observed that, in the SWIR image, a curl on the top of the head, later hidden by the green comb, appears. In Figure 9c,d, the homogeneity and distribution of a pigment—lead white—in the *Woman in an armchair* is assessed by applying the spectral classification Spectral Angle Mapping (SAM) algorithm and a reference spectrum from the analyzed painting.

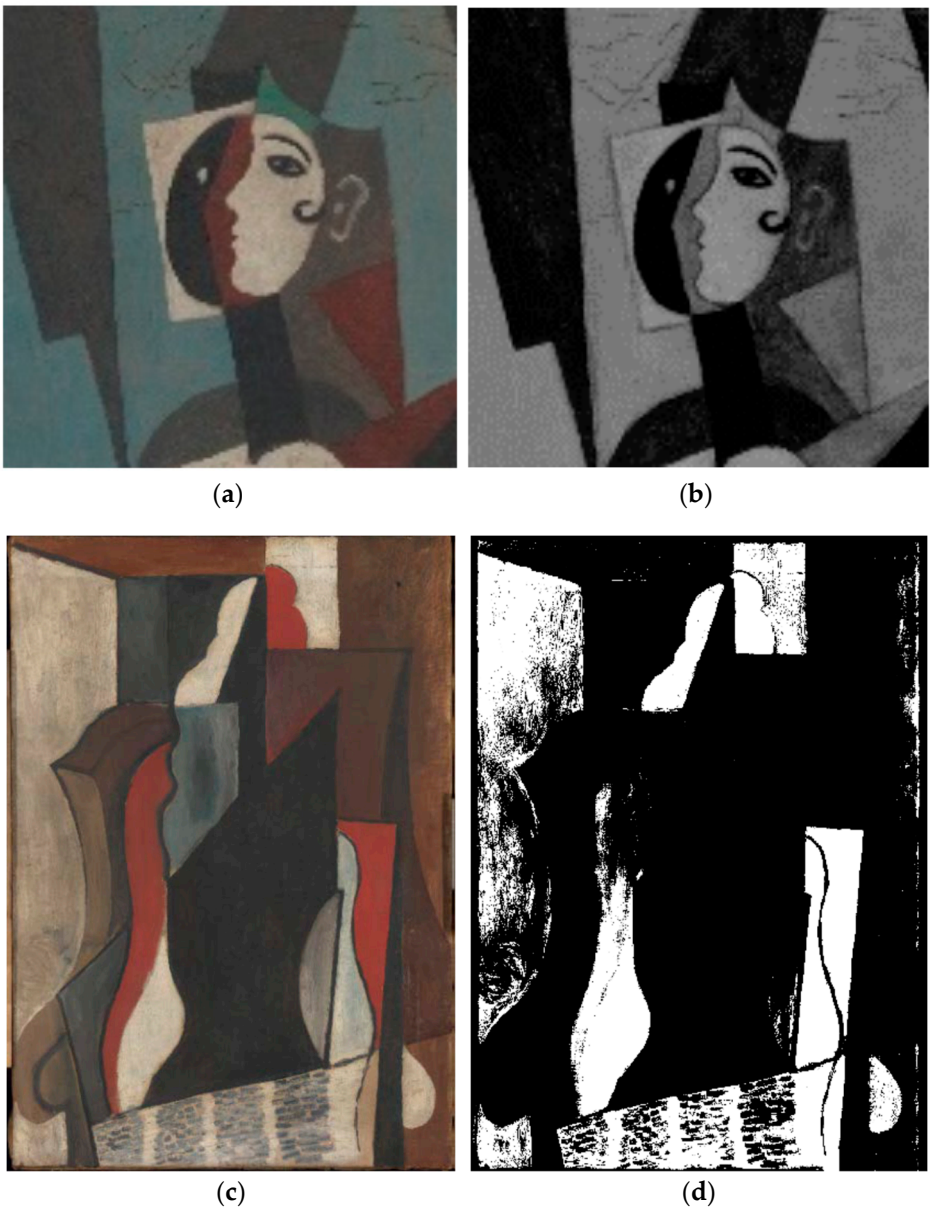

Figure 9. Hyperspectral imaging of modern paintings: *Blanquita Suárez* Picasso's painting—face detail sRGB image (**a**) and SWIR image at 1350 nm (**b**). Reconstructed sRGB image of *Woman in an armchair* painting from the HSI data (**c**) and Spectral Angle Mapping (SAM) distribution map of the lead white pigment (**d**) [62].

Another application of HSI is the analysis of historic texts and manuscripts, as well as of negative and positive photographic films. HSI data, indeed, allow for the identification of inks and pigments and, thus, they are useful for dating manuscripts [63] and recovering erased and overwritten scripts [64]. Moreover, HSI data are helpful to gather information about the conservation state of frames and provide spectroscopic information that may support their digital restoration, as discussed in [65], where further applicative examples are also reported. Furthermore, it is worth citing the use of HSI for mapping corrosion products on bronze sculptures (see e.g., [66]) and for investigating archeological walls with mural paintings and inscriptions (see [67]).

2.6. Terahertz Imaging (THz-TDI)

Imaging devices using radiation at wavelengths ranging from 30 μm to 3 mm can be considered as the newest among the diagnostic imaging tools and their more and more widespread use is owed to the non-ionizing nature of the THz waves and their penetration capability into dry, nonpolar, non-metallic materials, as well as the recent technological improvements that have allowed the commercialization of compact, flexible and portable systems [68].

In the past 20–30 years, THz imaging has experienced a rapid expansion that has allowed for the development of different imaging methodologies [69–71], among which is the "time of flight THz imaging" that enables a three-dimensional visualization of the internal structure of the investigated objects. Time of flight THz imaging provides information about position and thickness of inner layers as well as a geometrical characterization of hidden features. When focusing on artwork, there are several possibilities: (1) characterize texture and stratigraphy of materials; (2) detect, localize and visualize the shape of hidden defects or anomalies; (3) gather information on possible previous restoration actions [72]. All these goals are achieved without long term risks to the molecular stability of the exposed object and humans.

According to its potentiality, THz imaging has been used to investigate canvas, wall and copper paintings (see [73–76]). Several case studies have assessed its usefulness for characterizing the inner structure of paintings and gathering information on the preparation layers, which are difficult to achieve by means of XRR and IRR [72]. In addition, THz imaging has been exploited to characterize insect tunneling affecting wood carvings [77], as well as to study mummies [78,79].

A further example is represented by the analysis of ancient decorated mortar samples, such as that depicted in Figure 10a, which is dated back to the Roman Age and was found in the Urban Archeological Park of Piazza Municipio, Napoli, Italy. The THz images provided in Figure 10b–d have been obtained by exploiting the data processing strategy proposed in [80] and some results of a study presented at the European Geosciences Union assembly in 2020 [81]. Figure 10b,c shows the false color THz images representing, on each pixel, the maximum and minimum of the measured signal, respectively. These images reveal that the adopted red, green and black pictorial pigments have similar reflectivity, thus suggesting that they were made up of the same type of materials. Furthermore, the image in Figure 10c indicates the presence of a sub-superficial anomaly (outlined by the black circle). Furthermore, the radargrams referred to parallel measurement lines reveal the presence of three interfaces: (1) the pictorial layer; (2) the plaster used to make the mortar uniform; (3) the mortar; see Figure 10d, where a representative radargram is displayed.

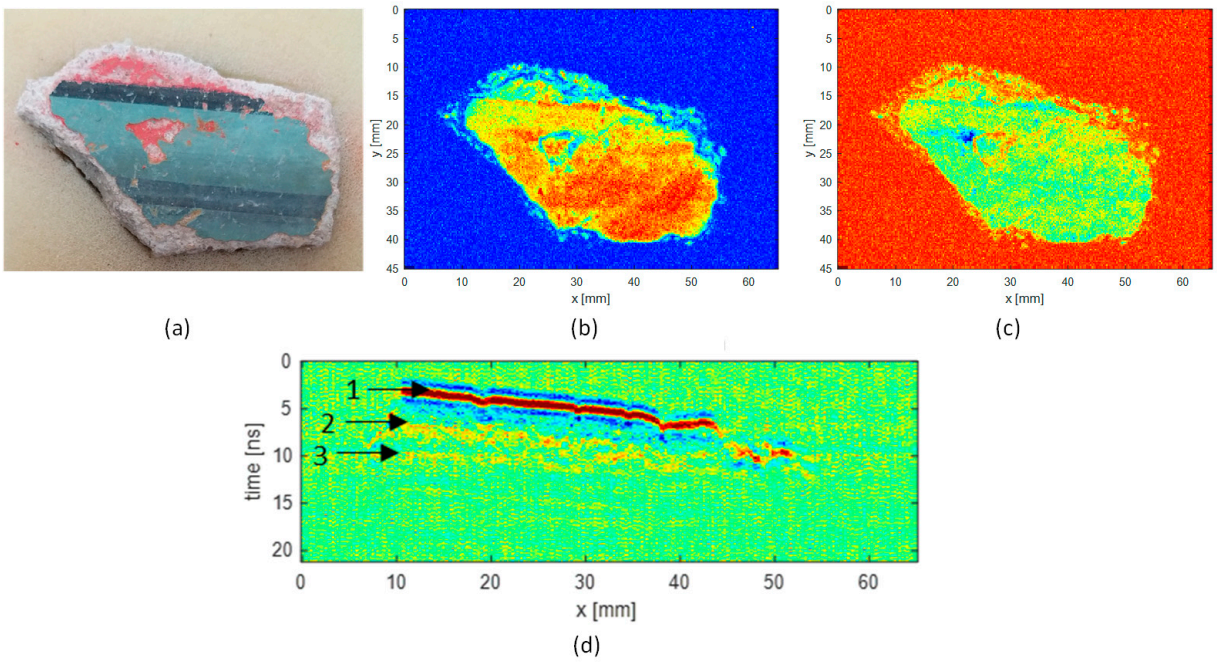

Figure 10. THz imaging of an ancient decorated mortar sample: (**a**) Optical image; (**b**) False color image showing the maximum of the collected signals; (**c**) False color image showing the minimum of the collected signals; (**d**) The representative radargram where the presence of pictorial (1), plaster (2) and mortar (3) layers is outlined by the numbered arrows. Adapted with permission from Catapano et al. 2020 [81]. Copyright the authors.

2.7. Integrated Techniques

The collaborative use of different technologies makes it possible to gather different pieces of information about the same object and, thus, it increases knowledge of the artwork history, from its realization phase to its current conservation state [19,40,82–84].

An example assessing the advantages offered by such synergistic exploitation is the case study presented in [19] regarding the Renaissance wall painting named *Annunciation*, painted by Fra Beato Angelico, which is visible in the Museum of San Marco (Florence, Italy). In this case study, both spot and imaging proximal sensing technologies, as well as digital imaging and GPR surveys, were performed but, herein, we consider the proximal sensing imaging techniques only and, specifically, UVF, IRR and THz-TDI. These techniques led to novel knowledge on the compositional scheme of the wall painting with regard to its stratigraphy and restoration. The UVF revealed the presence of small, almost dot-like areas, with pink fluorescence on Mary's gown. As the pink fluorescence is typical of red varnish, this result supports the hypothesis that, originally, Mary's gown was red-colored, differently from its current appearance. The IRR survey pointed out that these were not the artist's pentimenti and that the drawing was transferred onto the plaster by using the indirect incision technique, i.e., by positioning a one-to-one preparatory drawing and passing a point over the line of the drawing in order to leave the mark on the fresh plaster. Finally, THz-TDI, which was performed on some specific small areas, made it possible to detect repainted surface scratches, painted layers with different thicknesses and an elliptical-shaped inner discontinuity.

Figure 11 shows the wall painting, whose surface is 230 × 321 cm, and provides some of the above results.

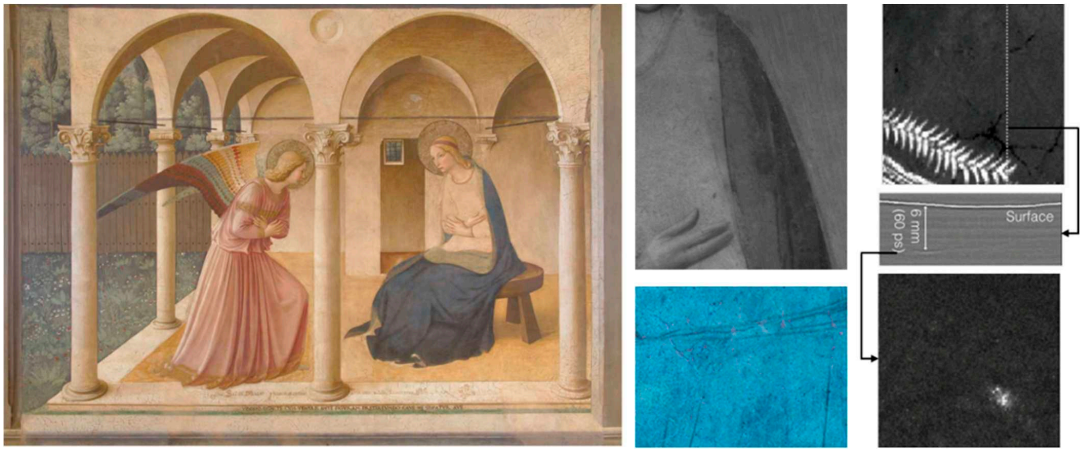

Figure 11. Combined use of proximal sensing imaging techniques: the case study of *Annunciation* wall painting by Fra Beato Angelico. Left panel: visible image of the painting. Middle upper panel: IRR results. Middle bottom panel: UVF result. Right panel: THz-TDI results. Adapted with permission from Catapano et al. 2020 [19]. Copyright 2019 Springer Nature B.V.

3. Micro-Geophysics

In the last decades, applied geophysics techniques have been oriented to very particular investigation targets of cultural heritage importance, keeping the benefit of advances in data acquisition and processing. A very important issue addressed by these innovative approaches has been the miniaturization of sensors and instrumentation to allow very detailed non-destructive study of medium-to-small items such as statues or historic architectural elements [85].

After some pioneering surveys [86–90], instrumental miniaturization has allowed the programmatic applications of geophysics to architectural elements since the end of the first decade of the 2000s [91–97].

Given the unifying importance of miniaturization, these methods and applications are commonly known as micro-geophysics [85]. The growing attention of our society to cultural heritage assets made possible a further extension of traditional disciplinary limits to innovative methods and technology which, even with strong contribution from consolidated geophysical techniques, are developed with the aim of resolving specific issues linked to the new diagnostic targets [95].

3.1. Microseismic, Sonic and Ultrasonic Surveys

The micro-geophysical approach implies the implementation of novel instrumental equipment and the use of source signals suitable to resolve defects and anisotropies of the materials, with high accuracy for a detailed inspection. The wavelength of the source signal is the main physical parameter which affects the resolution power of the non-invasive analyses.

In this framework, micro-seismic surveys concern the use of high-frequency acoustic signals (from 200 Hz to 20 kHz) and ultrasonic pulses (at frequencies greater than 20 kHz). The most frequently used source for sonic signals is the impact of a little hammer (impulsive signal) or a computerized sweep signal, transmitted through a sonic probe. The study of the velocity distribution of the wave field of both sonic and ultrasonic pulses into the media allows the indirect identification of the main elastic properties of the materials and the analysis of anomalous internal volumes, characterized by different size and shape [93,98]. The most common arrangements for sonic and ultrasonic surveys are based on the use of two signal probes (transmitter and receiver units) arranged on the surface of the medium with different geometrical configurations (direct, semi-direct and indirect tests). However, innovative and unconventional approaches provide more detailed information through the implementation of both sonic and ultrasonic multi-channel tomographies. The tomographic approach utilizes two-dimensional or three-dimensional

geometrical configurations of sensors and sources. Complex geometries of data acquisition allow the analysis of the internal volume of statues [99,100], architectural elements such as walls, pillars and columns [101,102] and the identification of internal artifacts and defects by means of the 3D reconstruction of the velocity field.

3.2. Electrical Surveys

Miniaturized electrical inspections consist of both passive (self-potential) and active (electrical resistivity and induced polarization) multi-pole surveys carried out through 2D and 3D arrays. The electrical resistivity models of the medium are derived from the solution of an inverse tomographic problem. The measurements are carried out through several acquisition schemes: single linear profiles, multiple parallel lines, three-dimensional arrays (U-shaped, L-shaped and other geometrical loops of electrodes). A main issue concerns the high contact impedance (up to 100 GΩ) of the target's surface in such measurements. In order to partially overcome this technical problem and to obtain a good coupling for the injection of the electrical current, several alternative types of electrodes have been tested (for instance, electrocardiography potential electrodes—ECGs). Since the resistivity values are strongly influenced by the presence of soluble salts and, therefore, of water, the resistivity models can be useful for reconstructing the humidity distribution model and any infiltration mechanisms [103]. Furthermore, electrical surveys can identify bodies or non-homogeneous volumes inside inspected assets due to their different resistivities. Moreover, resistivity surveys have been used to map the three-dimensional distribution of materials being injected into historic walls (mortar, resin, etc.), in order to enhance their resistance [104]. The method can provide excellent results also in the presence of saturated water with high salinity [105].

3.3. Electromagnetic Methods

Impulsive electromagnetic methods mainly include high-frequency ground penetrating radar (GPR) surveys. The central frequency of the radar systems, which are suitable to perform high-resolution non-destructive investigations, is usually greater than 1 GHz for such applications. Several configurations of data acquisition have been described in the literature: monostatic and bistatic modes, transmission and diffraction/reflection surveys. Different types of approaches can be used with high-frequency radar. The most common use of GPR creates profiles that show the reflections of the electromagnetic waves inside the investigated medium. The acquisition of multiple profiles enables the reconstruction of 2D maps and 3D volumes, which can highlight interpretable reflection geometries [106]. However, the small sizes of the targets normally analyzed in micro-geophysical applications, together with the possibility to illuminate the same studied volume through different or opposite sides of the object, encourage the use of tomographic investigations. First, arrival of the GPR signal transmitted through the medium is recorded. In fact, the travel times collected for numerous relative positions of the transmitter and receiver radar unit are affected by the geometrical features of the internal bodies and by the discontinuities present in the medium.

Electromagnetic induction (EMI) methods are sensible for identifying conductive anomalous bodies inside resistive media. EMI techniques include numerous methods and configurations of data acquisition and are classified according to the reciprocal geometrical disposition of the coils which compose the instrumental layout (transmitter and receiver coils) [107]. Micro-geophysical applications of EMI methods are mostly focused on moisture mapping and, in minor part, on detection and reconstruction of anomalous volumes with high contrast in physical properties (i.e., conductivity and magnetic susceptibility).

3.4. Architectural Elements Case Studies

Calcina et al. [108] used acoustic measurements to derive the velocity of longitudinal waves through the walls of two ancient twin bell towers to estimate the dynamic elastic modulus of the concrete and stone masonry. Thanks to these measurements, a Finite

Element model of the dynamic behavior of the religious complex was calibrated and compared with at-contact and remote vibration surveys.

More recently, an extensive experimental campaign was carried out on three leaf panels representative of existing masonry types, which were subjected to elastic wave transmission tests with various acquisition systems and data processing tools [109]. The panels were subjected to compression (P-type) and surface (Lamb–Rayleigh) waves by applying sonic and MASW (Multichannel Analysis of Surface Waves) tests, respectively. The specimens were studied in various configurations: (1) direct tests distributed on the main faces of the panels, (2) tomography applied to horizontal and vertical panel sections, (3) surface wave transmission tests along diagonals of panels. This study also established a framework for quantitative evaluation of the sonic pulse velocity characterizing various conditions detectable in representative masonry types. According to the authors, results were as follows:

- Sonic tests are effective in detecting large variations in the density of materials inside walls;
- Smaller inclusions can be identified, although still approximately, when crossed by tomographic sections or immersed in a high-density matrix, as in the case of effective consolidation of their surrounding incoherent material with grout injections;
- Both direct and tomographic tests confirmed their high reliability in quantifying the effectiveness of grout injections to homogenize consolidated inner cores with outer leaves;
- The surface wave transmission method was also effective in identifying the layered internal structure of the wall and the improvements provided by injection.

In the early days of micro-geophysics, a new application of GPR was proposed [89], presenting a framework of a high-resolution integrated project—including also petrographic analyses—to study patina growth (gypsum and calcium oxalate dihydrate) over calcarenitic blocks of monumental buildings. The authors observed that the amplitudes of the GPR waves reflected by the surfaces covered with gypsum and oxalate were systematically smaller than those from the areas that were patina-free (Figure 12). Furthermore, the waves reflected by the inner planes were characterized by lesser amplitudes when the patina was observed in the 1.4–2 GHz frequency range (Figure 13).

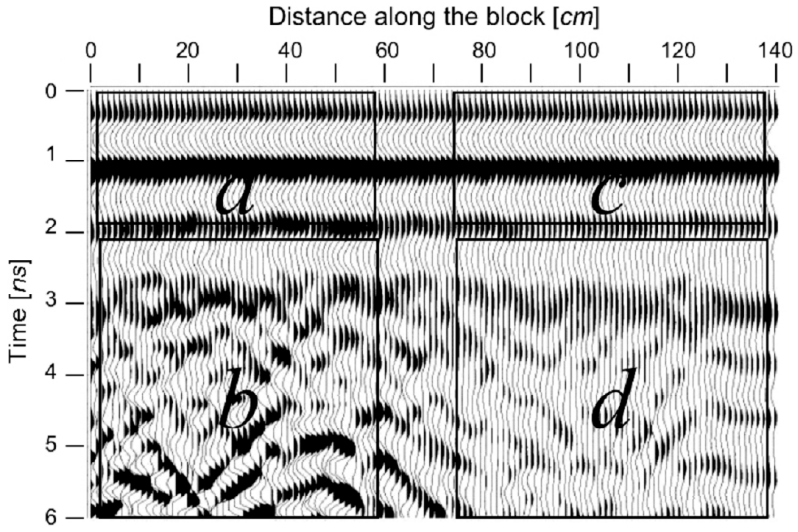

Figure 12. Typical radargram recorded over a wall affected by superficial patina: the profile crosses the separation between patina-free and patina-rich areas at about 65 cm. The spectral responses of the parts of signals contained in frames a, b, c and d are, respectively, presented in Figure 13. Reprinted with permission from Cosentino, and Deganello 2003 [89]. Copyright 2003 OGS.

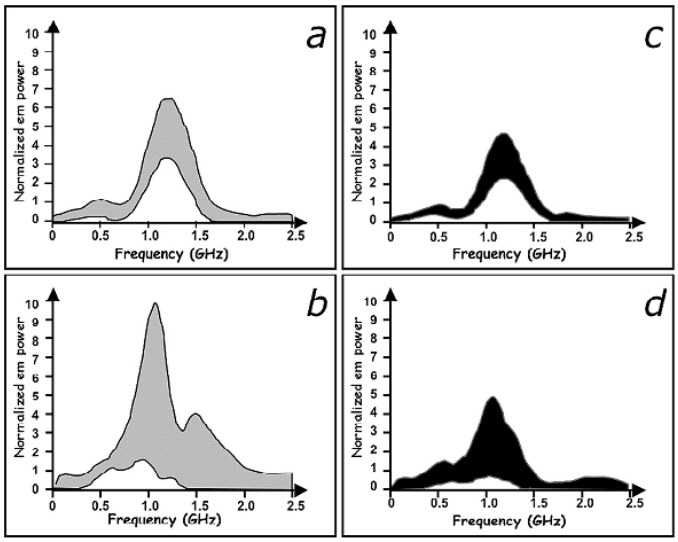

Figure 13. Spectral responses of parts of signals presented in Figure 12. Spectra (**a**,**b**) refer to patina-free areas, while (**c**,**d**) to patina-rich areas. It is to be noted that there is a damping in amplitude in d, especially in the 1.3–2.0 GHz frequency range. Reprinted with permission from Cosentino, and Deganello 2003 [89]. Copyright 2003 OGS.

Masini et al. [110] presented three case histories of ground penetrating radar (GPR) for the monitoring of historical building elements (i.e., a wall, a masonry pillar and a marble column) to evaluate different problems such as the characterization of the masonry, the detection of cracks and the imaging of metallic reinforcement bars. Two monostatic sets of antennae (1 GHz and 1.5 GHz) were used to perform the surveys. For the columns, twisted data were produced, starting from raw radargrams. Furthermore, B-scan data were, in some cases, inverted to obtain tomographic imaging across vertical sections of the columns.

Catapano et al. [111] illustrated the usefulness of GPR surveys enhanced using a microwave tomographic data processing approach as a methodology for the diagnosis and monitoring of CH exposed to climate events and natural hazards. Specifically, the paper reports on the results of a measurement campaign (2 GHz, monostatic) carried out at the Loggia of the Consoli Palace (Gubbio, Italy). The results allowed an improved knowledge of the construction modalities of the inspected masonry wall and the associated deterioration phenomena related to material aging and other structural issues. Thanks to the microwave tomography-enhanced GPR processing, the authors were able to estimate the depth of cracks, voids and of the inner stone layers (Figure 14(a1,b1)).

Recently [101], the Batalha Abbey, a late 14th century UNESCO building in central Portugal, was the target of an extensive geophysical survey that included also the micro-geophysical characterization of stone pillars and walls by means of GPR profiles (800 MHz, monostatic) and seismic tomography transmission (4.5 Hz geophones). In accordance with construction techniques used in the 14th century, it was expected that the inspected construction elements consisted of an outer layer of compact limestone blocks, whilst the interior could be filled with debris and lime mortar or cement. Given that GPR has higher resolution but poorer penetration depth and that seismic tomography, on the contrary, provides larger depths of penetration but poorer resolution, these two techniques are mutually complementary. Velocity analysis on pairs of GPR profiles—acquired along opposite sides of the 1.4 m thick columns to consider signal attenuation—was performed by hyperbola fitting and allowed the authors to define the constitutive layers' thicknesses and their relative dielectric permittivities. Instead, seismic tomography allowed the reconstruction of the elastic modulus variations across the pillar sections, highlighting transversal layering. Also, some local superficial areas of minimum P-wave velocity values were explained by the authors as being caused by superficial alteration of the limestone (visible at the

columns' surfaces), open joints between the limestone blocks (also observed locally) and the decompression of the limestone blocks near the surface.

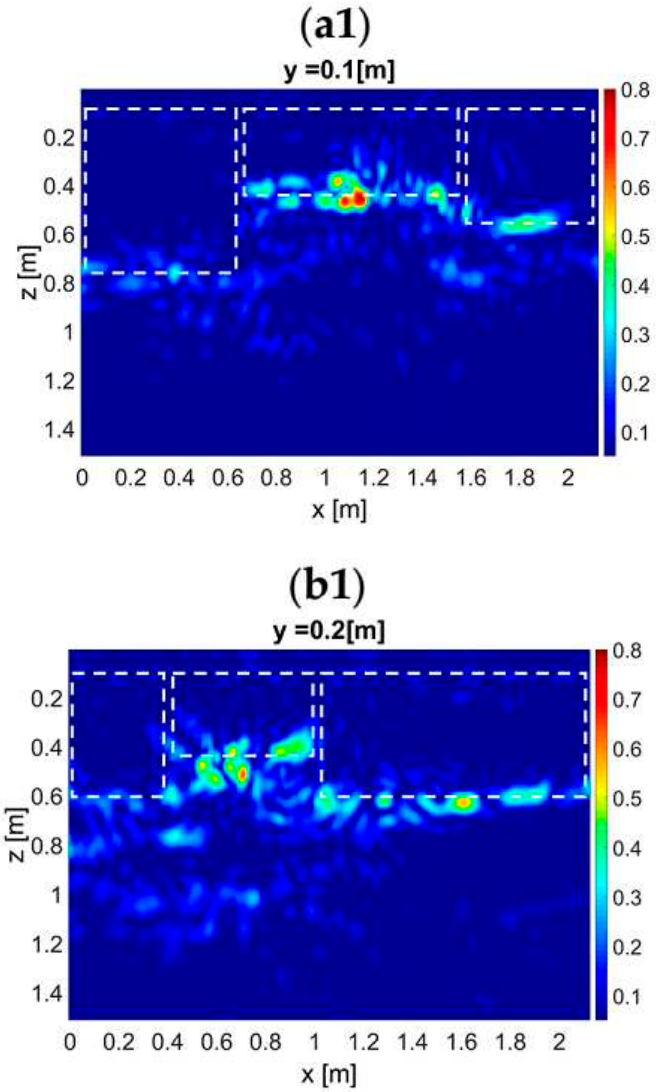

Figure 14. Tomographic images of the internal structures of the walls of the Consoli Palace of Gubbio, obtained from zero-offset GPR acquisitions and referred to the acquisition line at y = 0.1 m (**a1**) and y = 0.2 m (**b1**) in the local reference system of the prospection. The white dashed rectangles indicate the section of the masonry blocks of the inspected wall [111].

Another example relates to the investigation of the mosaics of Delos Island that are inscribed in UNESCO's World Heritage List. GPR systems (1600 MHz, 500 MHz and 250 MHz) have been used to evaluate the stratigraphic condition of the mosaic at House of the Dolphins which decorates the peristyle impluvium [112]. The 1.6 GHz system showed the best performance to identify the boundaries of the mosaic layers as well as the problematic areas, such as bulges and areas with high levels of moisture that may cause deterioration (Figure 15). The results obtained from the 500 MHz and 250 MHz survey proved to be complementary to the ones obtained from the high frequency system, as the emitted signals could reach deeper levels. Structural characteristics of the cistern below the main mosaic floor were mapped in some detail, including five stone arches.

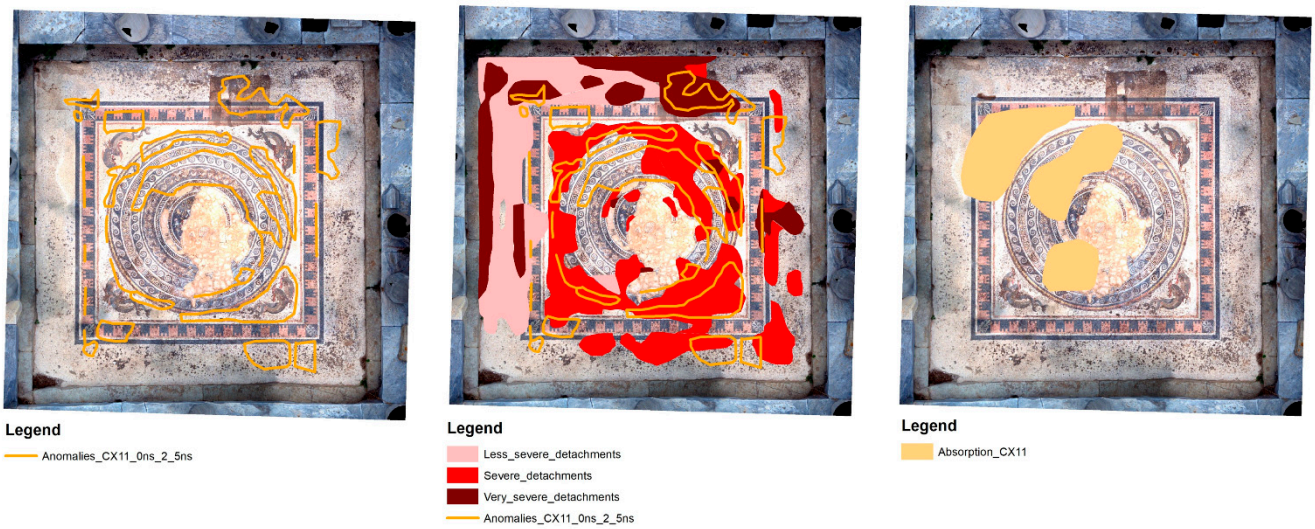

Figure 15. Detachment and absorption areas on the mosaics of Delos (Greece), detected by high-frequency GPR data analysis Adapted with permission from Manataki et al. 2019 [112]. Copyright 2019 EAGE Publications.

Electric resistivity tomography (ERT) is not a common method for studying precious walls and surfaces (such as floors with fresco or mosaic cladding), due to the high contact resistance which reduces current injection intensities. In fact, to obtain a good signal-to-noise ratio, it would be necessary to use small nails as electrodes. Fiandaca et al. [113] proposed an interesting application of the MYG array (which significantly reduces, compared to other classical arrays, the number of electrodes used for current injection) on a wall covered with mosaics, to investigate the cause of internal humidity.

Cardarelli et al. [114] applied an integrated approach to assess the condition of an ancient Roman building at the Ostia Antica archaeological site (Italy) that was affected by rising dampness and masonry cracking. Its state of conservation was studied using miniaturized and high-resolution seismic and ERT. Foundation works were analyzed with ERT to constrain bordering moisture conditions of an inner wall in *opus caementicium* that was instead investigated with the integrated micro-geophysical approach and validated by biological information on the exposed surfaces.

On a pillar of the church of San Giuseppe Calasanzio in Cagliari, Piroddi et al. [115] performed an integrated micro-geophysical study based on miniaturized ERTs and high-frequency GPR. ERTs were performed in a 2D fashion on the opposite sides of the pillar (with electrodes made of wet sponges) and in a cross-wall configuration (with thin stainless steel electrodes). GPR datasets were acquired along profiles on three sides of the pillar (2 GHz, monostatic) and in a transillumination tomographic set-up (1.7 GHz, bistatic). The joint inversion of Dipole–Dipole and Wenner–Schlumberger datasets allowed imaging of the stones of the pillar (dark red, high resistive patterns) and the joints between them (orthogonal to the electrodes lines, light red and orange tones, mid-resistive). Also, a probable rising moisture ramp (trend to conductive in the lower and internal parts of the pillar) that was not yet recognizable at the free surfaces was imaged (Figure 16). Conversely, the GPR profiles were able to better highlight the stone joints parallel to the acquisition surfaces.

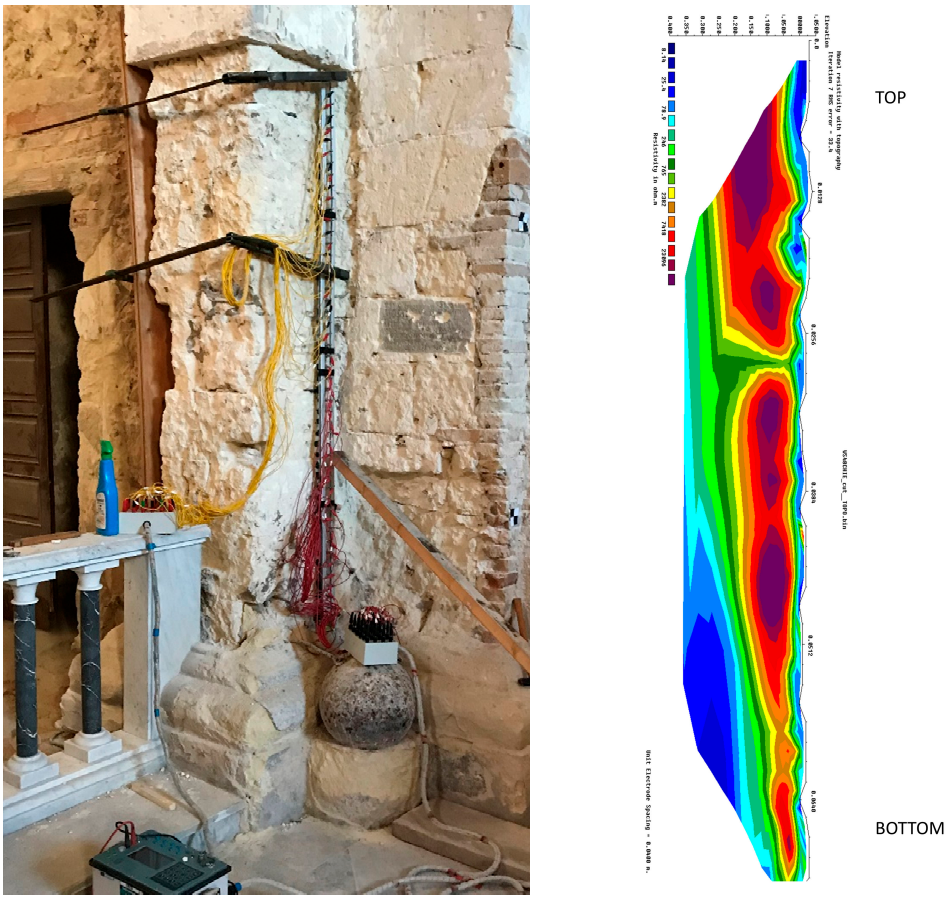

(**a**) (**b**)

Figure 16. The acquisition setup of the ERT datasets along the pillar of the church of San Giuseppe Calasanzio in Cagliari (Italy) (**a**); joint inversion of Dipole–Dipole and Wenner–Schlumberger datasets (**b**), that images the stones of the pillar and the joints between them and, also, a probable rising moisture ramp, not recognizable at the free surfaces. Adapted with permission from Piroddi et al. 2018 [115]. Copyright 2018 IEEE.

The integrity of the rose window of the Troia Cathedral, a precious Romanesque monument in southern Italy, against the development of cracks and distortions caused by past earthquakes was verified using high-frequency GPR systems (mainly 1.5 GHz monostatic) [116]. GPR was employed in the classical continuous reflection mode, moving the antennae manually along the architectural elements and paying exceptional care in the acquisition and processing stages to avoid positioning errors. Indeed, the challenging aspects of this case study were the geometrical complexity and small dimensions of the structural elements, causing many logistic/coupling problems [116]. From GPR data interpretation, based on signal analysis and correlation with features detected by visual inspection of the external surfaces, the diagnostic survey provided useful information on the internal structure of the rose window, detecting fractures and boundaries of previously restored parts and locating hidden metallic components connecting the architectural elements.

3.5. Statue Case Studies

In a programmatic collection of micro-geophysical applications, Cosentino et al. [85] also presented the 3D ultrasonic tomography carried out on the bust of Eleonora d'Aragona (sculptured by F. Laurana, 1468, Figure 17), finely carved from a block of white and microcrystalline marble. The survey was suggested by the discovery, during the cleaning of the sculpture, of a fracture in the central portion of the neck, involving the whole face of the lady, that probably originated on a natural veining of the marble block [85]. One

hundred fifty-seven measuring points, spaced 2–5 cm, were placed on the statue surface. Transmitter and receiver probes were characterized by a central frequency of 55 kHz. The model did not show significant discrepancies at the lesion on the face of the lady. Also, the upper torso (head and neck) showed velocity values corresponding to a sufficiently homogeneous and well-preserved marble. Low velocity values were found in the lower front portion of the trunk, corresponding to the support of the statue.

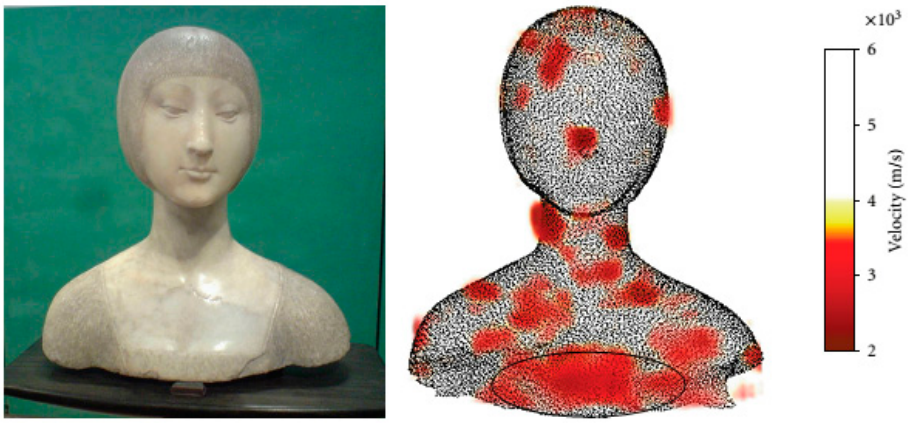

Figure 17. (**Left**) Bust of Eleonora d'Aragona (F. Laurana, 1468). (**Right**) Frontal 3D image with transparency of the investigated volume showing an area characterized by low P-wave velocity (or acoustic), corresponding to the support point of the bust [85].

The importance of a proper 3D geometrical reconstruction for a reliable ultrasonic tomographic characterization of precious and ancient statues is stressed in Donadio et al. [117], where the authors presented the results of a 3D ultrasonic tomography of the Egyptian *naophorous* statue of Amenmes and Reshpu, dated to the reign of Ramses II (1279–1213 BC) or later. The statue—dedicated to the gods Osiris, Isis and Horus—was affected by material (limestone) deterioration which consisted of material chips and cracks, especially on the inscribed base. Geometric reconstruction was based on photogrammetric and laser acquisition. The 3D ultrasonic tomography was concentrated on the lower part of the statue, with 71 measuring points and a pulse generator centered on 50 kHz. The achieved results proved that around 40% of the volume of the sculpture base presented a state of conservation that was particularly worrying, since the overall measured average velocity was lower than 1500 m/s due to damage and fractures (Figure 18).

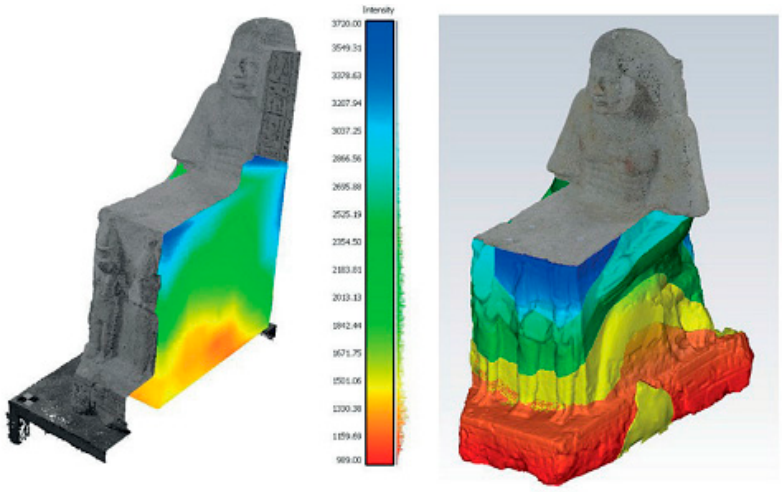

Figure 18. Improved representation of average velocities in the volume the Ramessid statue and the closed mesh extracted from the classified point cloud [117].

Cozzolino et al. [118] showed the results of a joint survey (photogrammetry and GPR) for the study and documentation of a stone trapezophoros with two griffins attacking a doe. The combined use of a 3D geometric survey and GPR analysis allowed assessment of the conservation condition of the trapezophoros. The creation of a high-resolution 3D model and the extraction of detailed orthophotos of the external surfaces through a photogrammetry digital survey were useful for documenting each sign of decay, even those that were not perceivable by the naked eye, and GPR radargrams showed their inner extents, allowing three new probable fractures to be identified (Figure 19).

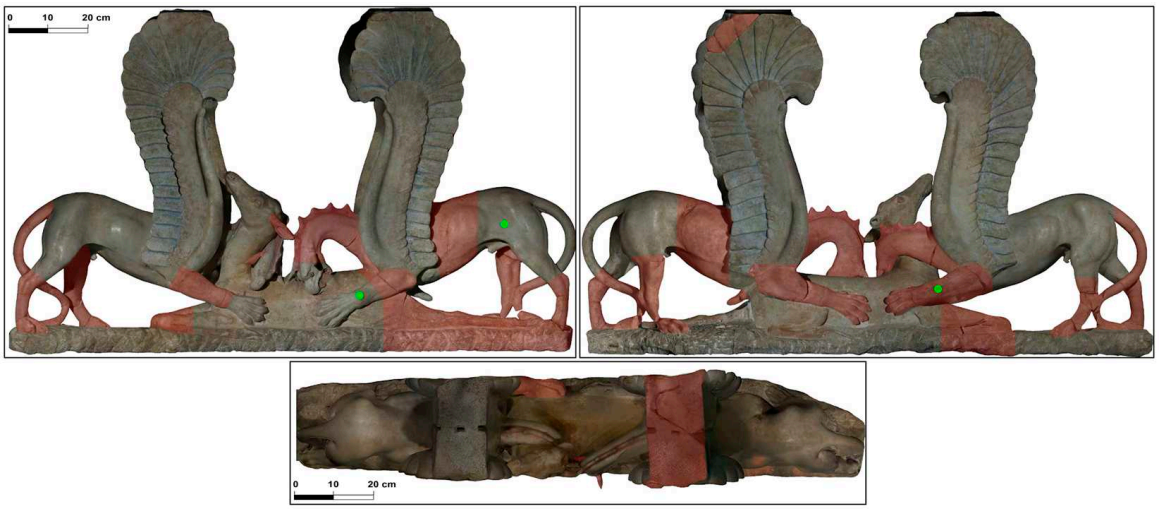

Figure 19. Indication of the areas more vulnerable to cracking phenomena, recognized by means of integrated photogrammetry and GPR surveys: front side, back side and top side [118].

Cosentino et al. [91] implemented different integrated and unconventional methods in the field of micro-geophysics for the non-destructive diagnosis and control of materials and human artifacts in civil engineering studies and in cultural heritage conservation. Different tomographic approaches have been tested for the reconstruction of two-dimensional and three-dimensional physical models. The authors used different energy sources during the experiments to analyze the wave propagation (sonic and ultrasonic) throughout the surveyed medium. The use of both sonic and ultrasonic frequency ranges was aimed at acquiring data with different resolution and depth of investigation. Methods and instrumental configurations suitable for the analyses of objects of small size were improved by enhancing the resolution of each survey. The authors proposed the "sonic imprint" corresponding to the sonic frequency response of the object [119]. The sonic imprint was suggested to characterize valuable artifacts (ancient Greek statues, unbroken and cracked plates, vessels and other cultural heritage artifacts). This method used piezoelectric probes arranged in arrays to acquire sonic signals produced by means of the impact of a small hammer on pre-established superficial points. The impact of the hammer excited the natural modes of vibration of the object. The experimental damped free vibration frequency analysis was used to derive a bar code (sonic imprint) which identified the specific response of the object.

3.6. Small Archaeological Features Case Studies

High-resolution geophysics has recently become of interest even for archaeological and paleontological studies, especially for the reconstruction of human and megafauna interactions by means of their fossil footprints. Urban et al. [120] successfully detected and imaged these kinds of footprints, even in cases of simultaneous presence (specifically, sloths, humans and mammoths), using GPR (central frequency 250 MHz, inter-line distance 12.5 cm). They occurred on an extensive gypsum playa, the erosional relict of ancient Lake Otero, dating from the Upper Pleistocene, and were intermittently and partially covered

by drifting sand. Using GPR data, they found that track density and faunal diversity may have been much greater than realized by the unaided human eye. From the biggest excavated footprints, they recorded the 3D surfaces and correlated them with the mean plantar pressure from African elephants retrieved from literature (Figure 20a).

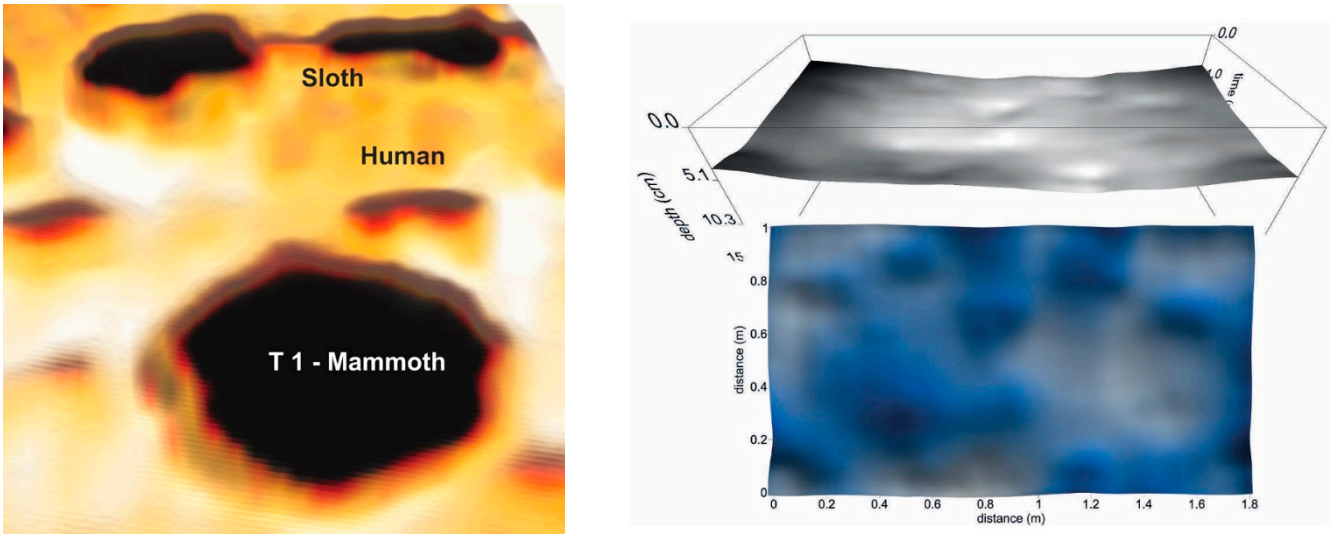

(**a**) (**b**)

Figure 20. Close up 3D GPR perspective of mammoth track 1 (T 1) along with human and sloth tracks. The presence of sloth tracks was not known prior to the GPR survey and was later confirmed when the prints became partially visible after a period of precipitation (**a**) [120]. Three-dimensional trackway surface generated with horizon detection methods applied to a very high-resolution GPR dataset and the same result following subtraction of the trend surface (**b**) [121].

More recently, Wiewel et al. [121] studied a real-scale model of buried human footprints, to stress the capability of GPR in such an imaging goal, and they produced a 3D image of the clay soil interface containing the footprints with a horizon detection processing technique. The final experimental dataset was collected with an antenna of 2.6 GHz nominal frequency and 10 cm of interline distance, but even 900 MHz and 2 GHz systems were tested. They concluded that the 2.6 GHz was the ideal solution for an archaeological layer at an approximate depth of 5.5–6.5 cm below the ground surface for the typical dimensions of the human footprints, while tuning the correct spatial sampling frequency is considered a very important parameter. In fact, the interline distance of 10 cm, used for data acquisition, revealed most but not all the footprints. To overcome this limitation, authors suggested increasing line density or using appropriate multichannel arrays (Figure 20b).

The effectiveness of the magnetic method was demonstrated by Urban et al. [122] for identifying the Pleistocene Megafauna tracks at White Sands National Monument in New Mexico. The presence of iron staining and salt concentration at the base of many of the tracks produced, indeed, a weak magnetic anomaly (<2 nT) that allowed the detection of their presence with magnetometry. Furthermore, Urban et al. [123] adopted the methodology for investigating some archaeological sites ranging from the terminal Pleistocene to historic periods located at high latitudes. Their results, obtained at the site of Swift Water Place in Alaska (USA), where magnetic measurements were integrated with GPR and electromagnetic induction data, allowed the identification of the locations of small, buried hearths.

4. Concluding Remarks

At the small scale, the analyzed surveying applications of heritage manufacts present some differences between proximal sensing and micro-geophysical techniques. In fact, in

the case of micro-geophysics, the appealing resort to integrated diagnostics is still more frequent than in the case of proximal sensing applications. This is probably partially due to the fact that micro-geophysical investigation methods—despite the various physical parameters reconstructed and the subsequently different physical laws exploited—are gathered by their common origin from a wider discipline (applied geophysics), from which they largely keep updated expertise and hardware and software solutions, that need only to be customized to suit the specific problems to solve. The general organization of geophysical laboratories as multi-method sets, jointly with the large number of unknown parameters to be retrieved in volumetric inspections, have led to integrated surveys since the first investigations. Conversely, proximal sensing and contactless applications, at similar scales, more often present a deep specialization in the disciplinary advancements and reserve integrated analyses for specific diagnostic problems for each artifact. In these cases, integrated diagnostics are nowadays frequently achieved by the parallel activity of multiple teams, even in long-lasting and complex projects for the knowledge of very precious heritage assets. Despite these differences, mostly linked to the different technological specializations of each family of techniques, contact and contactless methods present—at a small and homogeneous scale—many common procedures, especially in image reconstruction and post-processing.

Author Contributions: Conceptualization, L.P.; writing—original draft preparation, L.P., S.V.C., L.C. and I.C.; writing—review and editing, L.P., N.A.Z., S.V.C., P.C., L.C., I.C., M.C., S.D., R.L. and D.T.; supervision, L.P. All authors have read and agreed to the published version of the manuscript.

Funding: S.D. has been partially supported by the project ADVANCED E-LEARNING FOR CULTURAL HERITAGE RESTORERS SPECIALISATION (ADELE -RS), funded by the Erasmus+ European Programme—Action KA220 VET programme.

Data Availability Statement: No new data were created for this article.

Conflicts of Interest: The authors declare no conflict of interest.

References

1. Mairinger, F. UV-, IR- and X-ray- imaging. In *Non-Destructive Microanalysis of Cultural Heritage Materials*; Janssens, K.H.A., Grieken, R., Eds.; Wilson & Wilson Elsevier: Antwerp, Belgium, 2004; pp. 15–73.
2. Van Asperen de Boer, J.R.J. Infrared reflectography: A method for the examination of paintings. *Appl. Opt.* **1968**, *7*, 1711–1714. [CrossRef]
3. Aldrovandi, A.; Bertani, D.; Cetica, M.; Matteini, M. Multispectral image processing of paintings. *Stud. Conserv.* **1988**, *33*, 154–159.
4. Schreiner, M.; Frühmann, B.; Jembrih-Simbürger, D.; Linke, R. X-rays in art and archaeology: An overview. *Powder Diffr.* **2004**, *19*, 3–11. [CrossRef]
5. Saunders, D.; Billinge, R.; Cupitt, J.; Atkinson, N.; Liang, H. A new camera for high-resolution infrared imaging of works of art. *Stud. Conserv.* **2006**, *51*, 277–290. [CrossRef]
6. Hackney, S.; Townsend, J. Methods of examination and analysis. In *Paint and Purpose—A Study of Technique in British Art*; Hackney, S., Jones, R., Townsend, J., Eds.; Tate Gallery Publishing: London, UK, 1999; pp. 17–24.
7. Striova, J.; Ruberto, C.; Barucci, M.; Blažek, J.; Kunzelman, D.; Dal Fovo, A.; Fontana, R. Spectral imaging and archival data in analysing Madonna of the Rabbit paintings by Manet and Titian. *Angew. Chem. Int.* **2018**, *57*, 7408–7412. [CrossRef] [PubMed]
8. Liang, H. Advances in multispectral and hyperspectral imaging for archaeology and art conservation. *Appl. Phys.* **2012**, *106*, 309–323. [CrossRef]
9. Cucci, C.; Delaney, J.K.; Picollo, M. Reflectance hyperspectral imaging for investigation of works of art: Old master paintings and illuminated manuscripts. *Acc. Chem. Res.* **2016**, *49*, 2070–2079. [CrossRef]
10. Delaney, J.K.; Zeibel, J.G.; Thoury, M.; Littleton, R.; Palmer, M.; Morales, K.M.; de la Rie, E.R.; Hoenigswald, A. Visible and infrared imaging spectroscopy of Picasso's harlequin musician: Mapping and identification of artist materials *in Situ*. *Appl. Spectrosc.* **2010**, *64*, 584–594. [CrossRef]
11. Mounier, A.; Daniel, A. Hyperspectral imaging for the study of two thirteenth-century italian miniatures from the marcadé collection, treasury of the saint-andre cathedral in bordeaux, france. *Stud. Conserv.* **2015**, *60*, S200–S209. [CrossRef]
12. Cucci, C.; Webb, E.K.; Casini, A.; Ginanni, M.; Prandi, E.; Stefani, L.; Vitorino, T.; Picollo, M. Short-wave infrared reflectance hyperspectral imaging for painting investigations: A methodological study. *J. Am. Inst. Conserv.* **2019**, *58*, 16–36. [CrossRef]
13. Cucci, C.; Bracci, S.; Casini, A.; Innocenti, S.; Picollo, M.; Stefani, L.; Rao, I.G.; Scudieri, M. The illuminated manuscript Corale 43 and its attribution to Beato Angelico: Non-invasive analysis by FORS, XRF and hyperspectral imaging techniques. *Microchem. J.* **2018**, *138*, 45–57. [CrossRef]

14. Casini, A.; Bacci, M.; Cucci, C.; Lotti, F.; Porcinai, S.; Picollo, M.; Radicati, B.; Poggesi, M.; Stefani, L. Fiber optic reflectance spectroscopy and hyper-spectral image spectroscopy: Two integrated techniques for the study of the Madonna dei Fusi. In *Optical Methods for Arts and Archaeology*; Salimbeni, P., Ed.; SPIE: Bellingham, WA, USA, 2005; Volume 5857, p. 58570M-1-8.
15. Janssens, K.; Dik, J.; Cotte, M.; Susini, J. Photon-based techniques for nondestructive subsurface analysis of painted cultural heritage artifacts. *Acc. Chem. Res.* **2010**, *43*, 814–825. [CrossRef] [PubMed]
16. Romano, F.P.; Caliri, C.; Nicotra, P.; Di Martino, S.; Pappalardo, L.; Rizzo, F.; Santos, H.C. Real-time elemental imaging of large dimension paintings with a novel mobile macro X-ray fluorescence (MA-XRF) scanning technique. *J. Anal. At. Spectrom.* **2017**, *32*, 773–781. [CrossRef]
17. Fukunaga, K.; Picollo, M. Characterisation of works of art. In *Terahertz Spectroscopy and Imaging*; Peiponen, K.E., Zeitler, A., Kuwata-Gonokami, M., Eds.; Springer: Berlin/Heidelberg, Germany, 2013; Volume 171, pp. 521–538.
18. Pastorelli, G.; Trafela, T.; Taday, P.F.; Portieri, A.; Lowe, D.; Fukunaga, K.; Strlič, M. Characterisation of historic plastics using terahertz time-domain spectroscopy and pulsed imaging. *Analy. Bioanal. Chem.* **2012**, *403*, 1405–1414. [CrossRef] [PubMed]
19. Catapano, I.; Ludeno, G.; Cucci, C.; Picollo, M.; Stefani, L.; Fukunaga, K. Noninvasive analytical and diagnostic technologies for studying early renaissance wall paintings. *Surv. Geophys.* **2020**, *41*, 669–693. [CrossRef]
20. Gonzalez, V.; Cotte, M.; Vanmeert, F.; de Nolf, W.; Janssens, K. X-ray diffraction mapping for cultural heritage science: A review of experimental configurations and applications. *Eur. J. Chem.* **2020**, *26*, 1703–1719. [CrossRef]
21. Ravaud, E.; Pichon, L.; Laval, E.; Gonzalez, V.; Eveno, M.; Calligaro, T. Development of a versatile XRF scanner for the elemental imaging of paintworks. *Appl. Phys. A* **2016**, *122*, 17. [CrossRef]
22. Giudice, A.L.; Corsi, J.; Cotto, G.; Mila, G.; Re, A.; Ricci, C.; Sacchi, R.; Visca, L.; Zamprotta, L.; Pastrone, N.; et al. A new digital radiography system for paintings on canvas and on wooden panels of large dimensions. In Proceedings of the 2017 IEEE International Instrumentation and Measurement Technology Conference (I2MTC), Turin, Italy, 22–25 May 2017.
23. Impallaria, A.; Petrucci, F.; Chiozzi, S.; Evangelisti, F.; Squerzanti, S. A scanner for in situ X-ray radiography of large paintings: The case of "Paolo and Francesca" by G. Previati. *Eur. Phys. J. Plus* **2021**, *136*, 126. [CrossRef]
24. Re, A.; Albertin, F.; Avataneo, C.; Brancaccio, R.; Corsi, J.; Cotto, G.; De Blasi, S.; Dughera, G.; Durisi, E.; Ferrarese, W.; et al. X-ray tomography of large wooden artworks: The case study of "Doppio corpo" by Pietro Piffetti. *Herit. Sci.* **2014**, *2*, 19. [CrossRef]
25. Huppertz, A.; Wildung, D.; Kemp, B.J.; Nentwig, T.; Asbach, P.; Rasche, F.M.; Hamm, B. Nondestructive insights into composition of the sculpture of Egyptian queen Nefertiti with CT. *Radiology* **2009**, *251*, 233–240. [CrossRef]
26. Zesch, S.; Panzer, S.; Rosendahl, W.; Nance Jr, J.W.; Schönberg, S.O.; Henzler, T. From first to latest imaging technology: Revisiting the first mummy investigated with X-ray in 1896 by using dual-source computed tomography. *Eur. J. Radiol. Open* **2016**, *3*, 172–181. [CrossRef]
27. Aldrovandi, A.; Picollo, M. *Metodi di Documentazione e Indagini non Invasive sui Dipinti*; Il Prato: Padova, Italy, 2007.
28. Buzzegoli, E.; Keller, A. Ultraviolet fluorescence imaging. In *Scientific Examination for the Investigation of Paintings. A Handbook for Conservator-Restorers*; Pinna, D., Galeotti, M., Mazzeo, R., Eds.; Centro Di Edifimi srl: Firenze, Italy, 2009; pp. 204–206.
29. Dyer, J.; Verri, G.; Cupitt, J. Multispectral Imaging in Reflectance and Photo-Induced Luminescence Modes: A User Manual, Version 1.0. 2013. Available online: http://www.britishmuseum.org/pdf/charisma-multispectral-imaging-manual-2013.pdf (accessed on 11 March 2023).
30. Invernizzi, C.; Fichera, G.V.; Licchelli, M.; Malagodi, M. A non-invasive stratigraphic study by reflection FT-IR spectroscopy and UV-induced fluorescence technique: The case of historical violins. *Microchem. J.* **2018**, *138*, 273–281. [CrossRef]
31. Van Asperen de Boer, J.R.J. Reflectography of Paintings Using an Infrared Vidicon Television System. *Stud. Conserv.* **1969**, *14*, 96–118. [CrossRef]
32. Gavrilov, D.; Maev, R.; Almond, D.P. A review of imaging methods in analysis of works of art: Thermographic imaging method in art analysis. *Can. J. Phys.* **2014**, *92*, 341–364. [CrossRef]
33. Walmsley, E.; Metzger, C.; Delaney, J.K.; Fletcher, C. Improved Visualization of Underdrawings with Solid-state Detectors Operating in the Infrared. *Stud. Conserv.* **1994**, *39*, 217–231.
34. Casini, A.; Lotti, F.; Picollo, M.; Stefani, L.; Buzzegoli, E. Image Spectroscopy Mapping Technique for non-invasive Analysis of Paintings. *Stud. Conserv.* **1999**, *44*, 39–48. [CrossRef]
35. Poldi, G.; Villa, G.C.F. *Dalla Conservazione Alla Storia Dell'arte. Riflettografia e Analisi Non Invasive per lo Studio dei Dipinti*; Edizioni della Scuola Normale Publisher: Pisa, Italy, 2006.
36. Tucker, A.P. Infrared and Art: Using Infrared Photography in Art Conservation and History. Available online: https://irinfo.org/articles-2019/infrared-reflectography-5-1-19-tucker/ (accessed on 11 March 2023).
37. Kordatos, E.Z.; Exarchos, D.A.; Stavrakos, C.; Moropoulou, A.; Matikas, T.E. Infrared thermographic inspection of murals and characterization of degradation in historic monuments. *Constr. Build. Mater.* **2013**, *48*, 1261–1265. [CrossRef]
38. Glavaš, H.; Hadzima-Nyarko, M.; Haničar Buljan, I.; Barić, T. Locating hidden elements in walls of cultural heritage buildings by using infrared thermography. *Bldg* **2019**, *9*, 32. [CrossRef]
39. Biscarini, C.; Catapano, I.; Cavalagli, N.; Ludeno, G.; Pepe, F.A.; Ubertini, F. UAV photogrammetry, infrared thermography and GPR for enhancing structural and material degradation evaluation of the Roman masonry bridge of Ponte Lucano in Italy. *NDT E Int.* **2020**, *115*, 102287. [CrossRef]

40. Piroddi, L.; Catapano, I.; Colica, E.; D'Amico, S.; Galone, L.; Gargiulo, G.; Sfarra, S. The Pulcinella Diagnostic Project: Introduction to the Study of the Performances of Close-Range Diagnostics Targeted to a Wooden Physical Twin of a Carnival Historical Mask. In *Computational Science and Its Applications, Proceedings of the ICCSA 2022 Workshops, Malaga, Spain, 4–7 July 2022*; Springer International Publishing: Cham, Switzerland, 2022.
41. Mercuri, F.; Zammit, U.; Orazi, N.; Paolini, S.; Marinelli, M.; Scudeieri, F. Active infrared thermography applied to the investigation of art and historic artefacts. *J. Therm. Anal. Calorim.* **2011**, *104*, 475–485. [CrossRef]
42. Orazi, N. Mid-wave Infrared Reflectography and Thermography for the Study of Ancient Books: A Review. *Stud. Conserv.* **2020**, *65*, 437–449. [CrossRef]
43. Orazi, N. The study of artistic bronzes by infrared thermography: A review. *J. Cult. Herit.* **2020**, *42*, 280–289. [CrossRef]
44. Ibarra-Castanedo, C.; Sfarra, S.; Ambrosini, D.; Paoletti, D.; Bendada, A.; Maldague, X. Diagnostics of panel paintings using holographic interferometry and pulsed thermography. *Quant. InfraRed Thermogr. J.* **2010**, *7*, 85–114. [CrossRef]
45. Bendada, A.; Sfarra, S.; Ibarra, C.; Akhloufi, M.; Pradere, C.; Maldague, X. Subsurface imaging for panel paintings inspection: A comparative study of the ultraviolet, the visible, the in-frared and the terahertz spectra. *Opto-Electron. Rev.* **2015**, *23*, 90–101. [CrossRef]
46. Maldague, X.; Galmiche, F.; Ziadi, A. Advances in pulsed phase thermography. *Infrared Phys. Technol.* **2002**, *43*, 175–181. [CrossRef]
47. Sfarra, S.; Marcucci, E.; Ambrosini, D.; Paoletti, D. Infrared exploration of the architectural heritage: From passive infrared thermography to hybrid infrared thermography (HIRT) approach. *Mater. Construcción* **2016**, *66*, e094. [CrossRef]
48. Ceccarelli, S.; Guarneri, M.; Orazi, N.; Ferrucci, M.; Ciaffi, M.; Mercuri, F.; Paoloni, S.; Ferri de Collibus, M.; Zammit, U.; Petrucci, F. Remote and contactless infrared imaging tech-niques for stratigraphical investigations in paintings on canvas. *Appl. Phys. B* **2021**, *127*, 106. [CrossRef]
49. Cogoni, M. Nuove tecnologie non distruttive per lo studio e il restauro dei beni monumentali: Applicazioni termografiche e multispettrali nell'ipogeo di San Salvatore di Sinis in Cabras. Master's Thesis, University of Cagliari, Cagliari, Italy, 2015.
50. Piroddi, L.; Ranieri, G.; Cogoni, M.; Trogu, A.; Loddo, F. Time and spectral multiresolution remote sensing for the study of ancient wall drawings at San Salvatore hypogeum, Italy. In Proceedings of the 22nd European Meeting of Environmental and Engineering Geophysics, Near Surface Geoscience 2016, Barcellona, Spain, 4–8 September 2016.
51. Trogu, A.; Cogoni, M.; Ranieri, G.; Piroddi, L.; Loddo, F. Invisible but not lost. The recovery of the wall drawings of the hypogeum of San Salvatore di Sinis (Sardinia, Italy). In Proceedings of the 24th Annual Meeting of the European Association of Archaeologists, Barcelona, Spain, 5–8 September 2018.
52. Pelagotti, A.; Mastio, A.D.; Rosa, A.D.; Piva, A. Multispectral imaging of paintings. *IEEE Signal Process. Mag.* **2008**, *25*, 27–36. [CrossRef]
53. Piroddi, L.; Calcina, S.V.; Trogu, A.; Vignoli, G. Towards the definition of a low-cost toolbox for qualitative inspection of painted historical vaults by means of modified DSLR cameras, open source programs and signal processing techniques. In *Computational Science and Its Applications, Proceedings of the ICCSA 2020: 20th International Conference, Cagliari, Italy, 1–4 July 2020*; Springer International Publishing: Cham, Switzerland, 2020; pp. 971–991.
54. Easton, R.L.; Knox, K.T.; Christens-Barry, W.A. Multispectral imaging of the Archimedes palimpsest. In Proceedings of the 32nd Applied Imagery Pattern Recognition Workshop, Washington, DC, USA, 15–18 October 2003.
55. Hyperspectral Imaging for Art Conservation. Available online: https://surfaceoptics.com/applications/art-antiquities-conservation-hyperspectral/ (accessed on 7 March 2023).
56. Landgrebe, D. Information extraction principles and methods for multispectral and hyperspectral image data. *Inf. Process. Remote Sens.* **1999**, *82*, 3–37.
57. Du, Q.; Fowler, J.E. Low-complexity principal component analysis for hyperspectral image compression. *Int. J. High Perform. Comput. Appl.* **2008**, *22*, 438–448. [CrossRef]
58. Wang, J.; Chang, C.I. Independent component analysis-based dimensionality reduction with applications in hyperspectral image analysis. *IEEE Trans. Geosci. Remote Sens.* **2006**, *44*, 1586–1600. [CrossRef]
59. Bioucas-Dias, J.M.; Plaza, A.; Camps-Valls, G.; Scheunders, P.; Nasrabadi, N.; Chanussot, J. Hyperspectral remote sensing data analysis and future challenges. *IEEE Geosci. Remote Sens. Mag.* **2013**, *1*, 6–36. [CrossRef]
60. Plaza, A.; Benediktsson, J.A.; Boardman, J.W.; Brazile, J.; Bruzzone, L.; Camps-Valls, G.; Chanussot, J.; Fauvel, M.; Gamba, P.; Gualtieri, A. Recent advances in techniques for hyperspectral image processing. *Remote Sens. Environ.* **2009**, *113*, S110–S122. [CrossRef]
61. Cucci, C.; Casini, A. Hyperspectral imaging for artworks investigation. *Data Handl. Sci. Technol.* **2020**, *32*, 583–604.
62. Picollo, M.; Casini, A.; Cucci, C.; Stefani, L.; Jiménez-Garnica, R.; Fuster-López, L. Documentation and analysis of some Picasso's paintings by using hyper-spectral imaging technique to support their conservation and stylistic matters. *IOP Conf. Ser. Mater. Sci. Eng.* **2020**, *949*, 012023. [CrossRef]
63. Melessanaki, K.; Papadakis, V.; Balas, C.; Anglos, D. Laser induced breakdown spectroscopy and hyperspectral imaging analysis of pigments on an illuminated manuscript. *Spectrochim. Acta Part B* **2001**, *56*, 2337–2346. [CrossRef]
64. Balas, C.; Papadakis, V.; Papadakis, N.; Papadakis, A.; Vazgiouraki, E.; Themelis, G. A novel hyperspectral imaging apparatus for the nondestructive analysis of objects of artistic and historic value. *J. Cult. Herit.* **2003**, *4*, 330–337. [CrossRef]

65. Picollo, M.; Cucci, C.; Casini, A.; Stefani, L. Hyper-spectral imaging technique in the cultural heritage field: New possible scenarios. *Sensors* **2020**, *20*, 2843. [CrossRef]
66. Catelli, E.; Randeberg, L.Y.; Strandeberg, H.; Alsberg, B.K.; Maris, A.; Vikky, L. Can hyperspectral imaging be used to map corrosion products on outdoor bronze sculptures. *J. Spectr. Imaging* **2018**, *7*, a10. [CrossRef]
67. Cucci, C.; Picollo, M.; Chiarantini, L.; Uda, G.; Fiori, L.; De Nigris, B.; Osanna, M. Remote-sensing hyperspectral imaging for applications in archaeological areas: Non-invasive investigations on wall paintings and on mural inscriptions in the Pompeii site. *Microchem. J.* **2020**, *158*, 105082. [CrossRef]
68. Guillet, J.P.; Recur, B.; Frederique, L.; Bousquet, B.; Canioni, L.; Manek-Hönninger, I.; Desbarats, P.; Mounaix, P. Review of terahertz tomography techniques. *J. Infrared Millim. Terahertz Waves* **2014**, *35*, 382–411. [CrossRef]
69. Peiponen, K.E.; Kuwata-Gonokami, M.; Axel Zeitler, J. *Terahertz Spectroscopy and Imaging*; Springer: Berlin, Germany, 2013.
70. Herrmann, M.; Tani, M.; Sa-kai, K. Display modes in time-resolved terahertz imaging. *Jpn. J. Appl. Phys.* **2000**, *39*, 6254–6258. [CrossRef]
71. Saha, A. *Advances in Terahertz Imaging. Emerging Trends in Terahertz Solid-State Physics and Devices*; Springer: New York, NY, USA, 2020; pp. 143–168.
72. Fukunaga, K. *THz Technology Applied to Cultural Heritage in Practice (Cultural Heritage Science)*; Springer Nature AG: Cham, Switzerland, 2016.
73. Seco-Martorell, C.; López-Domínguez, V.; Arauz-Garofalo, G.; Redo-Sanchez, A.; Palacios, J.; Tejada, J. Goya's artwork imaging with Terahertz waves. *Opt. Express* **2013**, *21*, 17800–17805. [CrossRef] [PubMed]
74. Fukunaga, K.; Hosako, I.; Palazzo, M.; Dall'Aglio, L.; Aramini, F.; Cucci, C.; Picollo, M.; Ikari, T.; Duling, I.N. Terahertz time-domain imaging of "The Last Supper". In Proceedings of the 2020 45th International Conference on Infrared, Millimeter, and Terahertz Waves (IRMMW-THz), Buffalo, NY, USA, 8–13 November 2020.
75. Krügener, K.; Ornik, J.; Schneider, L.M.; Jäckel, A.; Koch-Dandolo, C.L.; Castro-Camus, E.; Riedl-Siedow, N.; Koch, M.; Viöl, W. Terahertz inspection of buildings and architectural art. *Appl. Sci.* **2020**, *10*, 5166. [CrossRef]
76. Cassar, Q.; Koch-Dandolo, C.L.; Guillet, J.P.; Roux, M.; Fauquet, F.; Perraud, J.B.; Mounaix, P. Characterization of Varnish Ageing and its Consequences on Terahertz Imagery: Demonstration on a Painting Presumed of the French Renaissance. *J. Infrared Millim. Terahertz Waves* **2020**, *41*, 1556–1566. [CrossRef]
77. Stübling, E.; Staats, N.; Globisch, B.; Schell, M.; Portsteffen, H.D.; Koch, M. Investigating the Layer Structure and Insect Tunneling on a Wooden Putto Using Robotic-Based THz Tomography. *IEEE Trans. Terahertz Sci. Technol.* **2020**, *10*, 343–347. [CrossRef]
78. Fukunaga, K.; Cortes, E.; Cosentino, A.; Stuenkel, I.; Leona, M.; Duling, I.N., III; Mininberg, D.T. Investigating the use of terahertz pulsed time domain reflection imaging for the study of fabric layers of an Egyptian mummy. *J. Eur. Opt. Soc.-Rapid Publ.* **2011**, *6*, 11040. [CrossRef]
79. Oehrstrom, L.; Bitzer, A.; Walther, M.; Ruhli, F.J. Technical note: Terahertz imaging of an-cient mummies and bone. *Am. J. Phys. Anthropol.* **2010**, *142*, 497–500. [CrossRef]
80. Catapano, I.; Soldovieri, F. A data processing chain for terahertz imaging and its use in artwork diagnostics. *J. Infrared Millim. Terahertz Waves* **2017**, *38*, 518–530. [CrossRef]
81. Catapano, I.; Noviello, C.; Ludeno, G. THz imaging in the frame of the Archaeological Urban Park of Naples project. In Proceedings of the EGU General Assembly 2020, Online, 4–8 May 2020.
82. van Loon, A.; Noble, P.; Krekeler, A.; Van der Snickt, G.; Janssens, K.; Abe, Y.; Nakai, I.; Dik, J. Artificial orpiment, a new pigment in Rembrandt's palette. *Herit. Sci.* **2017**, *5*, 26. [CrossRef]
83. Gabrieli, F.; Delaney, J.K.; Erdmann, R.G.; Gonzalez, V.; van Loon, A.; Smulders, P.; Berkeveld, R.; van Langh, R.; Keune, K. Reflectance imaging spectroscopy (Ris) for operation night watch: Challenges and achievements of imaging rembrandt's masterpiece in the glass chamber at the rijksmuseum. *Sensors* **2021**, *21*, 6855. [CrossRef] [PubMed]
84. Quintero Balbas, D.; Dal Fovo, A.; Montalbano, L.; Fontana, R.; Striova, J. Non-invasive contactless analysis of an early drawing by Raffaello Sanzio by means of optical methods. *Sci. Rep.* **2022**, *12*, 15602. [CrossRef] [PubMed]
85. Cosentino, P.L.; Capizzi, P.; Martorana, R.; Messina, P.; Schiavone, S. From Geophysics to Microgeophysics for Engineering and Cultural Heritage. *Inter. J. Geophys.* **2011**, *2021*, 428412. [CrossRef]
86. Ranieri, G.; Giani, G.P.; Ferrero, A.M. Indagini geofisiche sulle colonne del Duomo di Orvieto. *Semin. Geofis. L'archeologia* **1991**, *1*, 259–280.
87. Cardarelli, E.; Godio, A.; Jin, G.T.; Marrone, C.; Morelli, G.; Sambuelli, L.; Santarato, G.; Socco, L.V. Indagini geofisiche integrate alla volta della scarsella del battistero di s. Giovanni in Firenze. In Proceedings of the 18° Convegno annuale del Gruppo Nazionale Geofisica della Terra Solida, Consiglio Nazionale delle Ricerche, Rome, Italy, 9–11 November 1999; Volume 1, pp. 1–16.
88. Marchisio, M.; Onofrio, L.D.; Forlani, E.; Cerri, S. Diagnostica non pervasiva con metodologie dinamiche di origine geofisica sulle strutture murarie di edifici monumentali. *Sci. Technol. Cult. Herit.* **2001**, *10*, 41–62.
89. Cosentino, P.L.; Deganello, S. High-resolution microgeophysics: A fascinating challenge. I. Detection of thin patinas. *Boll. Geofis. Teor. Appl.* **2003**, *44*, 169–179.
90. Cosentino, P.L.; Martorana, R. Micro-geofísica de alta resolución: Tomografía eléctrica para muros High-resolution micro-geophysics: Electrical tomography for walls. In Proceedings of the 3rd Asamblea Hispano Portuguesa de Geodesia y Geofísica, Valencia, Spain, 4–8 February 2002; pp. 1794–1798.

91. Cosentino, P.L.; Capizzi, P.; Fiandaca, G.; Martorana, R.; Messina, P. Advances in micro-geophysics for engineering and cultural heritage. *J. Earth Sci.* **2009**, *20*, 626–639. [CrossRef]
92. Binda, L.; Lualdi, M.; Saisi, A.; Zanzi, L. Radar investigation as a complementary tool for the diagnosis of historic masonry buildings. *Int. J. Mater. Struct. Integr.* **2011**, *5*, 1–25. [CrossRef]
93. Martinho, E.; Dionísio, A. Main geophysical techniques used for non-destructive evaluation in cultural built heritage: A review. *J. Geophys. Eng.* **2014**, *11*, 053001. [CrossRef]
94. Ranieri, G.; Trogu, A.; Noli, L.M.; Sitzia, M.A.; Calcina, S.V.; Piroddi, L.; Loddo, F. Method and System for Activating and Controlling a Water-Repelling Process in Walls. European Patent EP3040490B1, 30 December 2014.
95. Piro, S.; Negri, S.; Quarta, T.A.M.; Pipan, M.; Forte, E.; Ciminale, M.; Cardarelli, E.; Capizzi, P.; Sambuelli, L. Geophysics and cultural heritage: A living field of re-search for Italian geophysicists. *First Break* **2015**, *33*, 43–54. [CrossRef]
96. Cardarelli, E.; De Donno, G.; Scatigno, C.; Oliveti, I.; Martinez, M.P.; Prieto-Taboada, N. Geophysical and geochemical techniques to assess the origin of rising damp of a Roman building (Ostia Antica archaeological site). *Microchem. J.* **2016**, *129*, 49–57. [CrossRef]
97. Arosio, D.; Hojat, A.; Munda, S.; Zanzi, L. High-Frequency GPR In-vestigations in Saint Vigilius Cathedral, Trento. In Proceedings of the 24th European Meeting of Environmental and Engineering Geophysics, European Association of Geoscientists & Engineers, Porto, Portugal, 9–12 September 2018; Volume 1, pp. 1–5.
98. Cardani, G.; Binda, L. Guidelines for the masonry quality evaluation in built heritage. In *BH2013-Built Heritage 2013 Monitoring Conservation Management*; Boriani, M., Garabaglio, R., Gulotta, D., Eds.; Politecnico di Milano, Centro per la Conservazione e Valorizzazione dei Beni Culturali: Milan, Italy, 2013; pp. 1–6.
99. Sambuelli, L.; Bohm, G.; Capizzi, P.; Cardarelli, E.; Cosentino, P. Comparison among GPR measurements and ultrasonic tomographies with different inversion algorithms. An application to the basement of an ancient Egyptian sculpture. *J. Geophys. Eng.* **2011**, *8*, S106–S116. [CrossRef]
100. Capizzi, P.; Cosentino, P.L.; Schiavone, S. Some tests of 3D ultrasonic traveltime tomography on the Eleonora d'Aragona statue (F. Laurana, 1468). *J. Appl. Geophys.* **2013**, *91*, 14–20. [CrossRef]
101. Matias, M.; Almeida, F.; Moura, R.; Barraca, N. High resolution NDT in the characterization of the inner structure and materials of heritage buildings walls and columns. *Constr. Build. Mater.* **2021**, *267*, 121726. [CrossRef]
102. Negri, S.; Aiello, M.A. High-resolution GPR survey for masonry wall diagnostics. *J. Build. Eng.* **2021**, *33*, 101817. [CrossRef]
103. Martinho, E.; Alegria, F.; Dionisio, A.; Grangeia, C.; Almeida, F. 3D-resistivity imaging and distribution of water soluble salts in Portuguese Renaissance stone bas-reliefs. *Eng. Geol.* **2012**, *141–142*, 33–44. [CrossRef]
104. Abu-Zeid, N.; Botteon, D.; Cocco, G.; Santarato, G. Non-invasive characterisation of ancient foundations in Venice using the elec-trical resistivity imaging technique. *NDT E Int.* **2006**, *39*, 67–75. [CrossRef]
105. Abu Zeid, N.; Balducci, M.; Bartocci, F.; Regni, R.; Santarato, G. Indirect estimation of injected mortar volume in historical walls using the Electrical Resistivity Tomography. *J. Cult. Herit.* **2010**, *11*, 220–227. [CrossRef]
106. Conyers, L.B. *Interpreting Ground-Penetrating Radar for Archaeology*; Routledge: Oxfordshire, UK, 2016.
107. Leucci, G. *Nondestructive Testing for Archaeology and Cultural Heritage: A Practical Guide and New Perspectives*; Springer: Berlin/Heidelberg, Germany, 2018.
108. Calcina, S.V.; Piroddi, L.; Ranieri, G. Vibration analysis of historic bell towers by means of contact and remote sensing measurements. *Nondestruct. Test. Eval.* **2016**, *31*, 331–359. [CrossRef]
109. Valluzzi, M.R.; Cescatti, E.; Cardani, G.; Cantini, L.; Zanzi, L.; Colla, C.; Casarin, F. Calibration of sonic pulse velocity tests for detection of variable conditions in masonry walls. *Constr. Build. Mater.* **2018**, *192*, 272–286. [CrossRef]
110. Masini, N.; Persico, R.; Rizzo, E. Some examples of GPR prospecting for monitoring of the monumental heritage. *J. Geophys. Eng.* **2010**, *7*, 190–199. [CrossRef]
111. Catapano, I.; Ludeno, G.; Soldovieri, F.; Tosti, F.; Padeletti, G. Structural assessment via ground penetrating radar at the Consoli Palace of Gubbio (Italy). *Remote Sens.* **2018**, *10*, 45. [CrossRef]
112. Manataki, M.; Maris, C.; Sarris, A.; Vafidis, A. Using GPR to Evaluate the Stratigraphic Condition of the Mosaic of the Dolphins in Delos Island, Greece, in order to Adopt the necessary Conservation measures. In Proceedings of the 10th International Workshop on Advanced Ground Penetrating Radar, European Association of Geoscientists & Engineers, The Hague, The Netherlands, 8–12 September 2019; Volume 1, pp. 1–7.
113. Fiandaca, G.; Martorana, R.; Messina, P.; Cosentino, P.L. 3D ERT for the study of an ancient wall covered by precious mosaics. In Proceedings of the Near Surface 2009—15th European Meeting of Environmental and Engineering Geophysics, Dublin, Ireland, 7–9 September 2009.
114. Cardarelli, E.; De Donno, G.; Scatigno, C. Three-dimensional reconstruction of a masonry building through electrical and seismic tomography validated by biological analyses. *Near Surf. Geophys.* **2018**, *16*, 53–65. [CrossRef]
115. Piroddi, L.; Vignoli, G.; Trogu, A.; Deidda, G.P. Non-destructive Diagnostics of Architectonic Elements in San Giuseppe Calasanzio's Church in Cagliari: A Test-case for Micro-geophysical Methods within the Framework of Holistic/integrated Protocols for Artefact Knowledge. In Proceedings of the 2018 Metrology for Archaeology and Cultural Heritage (MetroArchaeo), Cassino, Italy, 22–24 October 2018; pp. 17–21.
116. Masini, N.; Nuzzo, L.; Rizzo, E. GPR investigations for the study and the restoration of the Rose Window of Troia Cathedral (Southern Italy). *Near Surf. Geophys.* **2007**, *5*, 287–300. [CrossRef]

117. Donadio, E.; Spanò, A.; Sambuelli, L.; Picchi, D. Three-Dimensional (3D) modelling and optimization for multipurpose analysis and representation of ancient statues. In *Latest Developments in Reality-Based 3D Surveying and Modelling*; Remondino, F., Georgopoulos, A., Gonzalez-Aguilera, D., Agrafiotis, P., Eds.; MDPI: Basel, Switzerland, 2018; pp. 95–118.
118. Cozzolino, M.; Di Meo, A.; Gentile, V.; Mauriello, P.; Zullo, E. Combined Use of 3D Metric Survey and GPR for the Diagnosis of the Trapezophoros with Two Griffins Attacking a Doe of Ascoli Satriano (Foggia, Italy). *Geosciences* **2020**, *10*, 307. [CrossRef]
119. Cosentino, P.; Capizzi, P.; Fiandaca, G.; Martorana, R.; Messina, P.; Razo Amoroz, I. Identification of precious artefacts: The Sonic Imprint for small artefacts. *Curr. Anal. Chem.* **2010**, *6*, 111–117. [CrossRef]
120. Urban, T.M.; Bennett, M.R.; Bustos, D.; Manning, S.W.; Reynolds, S.C.; Belvedere, M.; Odess, D.; Santucci, V.L. 3-D radar imaging unlocks the untapped behavioral and biomechanical archive of Pleistocene ghost tracks. *Sci. Rep.* **2019**, *9*, 16470. [CrossRef]
121. Wiewel, A.; Conyers, L.; Piroddi, L.; Papadopoulos, N. An Experimental Use of Ground-Penetrating Radar to Identify Human Footprints. *Rev. D'archéométrie* **2021**, *45*, 1. [CrossRef]
122. Urban, T.M.; Bustos, D.; Jakeway, J.; Manning, S.W.; Bennett, M.R. Use of magnetometry for detecting and documenting multi-species Pleistocene megafauna tracks at White Sands National Monument, New Mexico, USA. *Quat. Sci. Rev.* **2018**, *199*, 206–213. [CrossRef]
123. Urban, T.M.; Rasic, J.T.; Alix, C.; Anderson, D.D.; Chisholm, L.; Jacob, R.W.; Manning, S.W.; Mason, O.K.; Tremayne, A.H.; Vinson, D. Magnetic detection of archaeological hearths in Alaska: A tool for investigating the full span of human presence at the gateway to North America. *Quat. Sci. Rev.* **2019**, *211*, 73–92. [CrossRef]